RADAR OBSERVATIONS OF MJO AND KELVIN WAVE INTERACTIONS DURING DYNAMO/AMIE/CINDY2011

A Thesis

by

AMANDA MICHELE DEPASQUALE

Submitted to the Office of Graduate Studies of
Texas A&M University
in partial fulfillment of the requirements for the degree of

MASTER OF SCIENCE

Chair of Committee,	Courtney Schumacher
Co-Chair of Committee,	Anita Rapp
Committee Member,	Mary Jo Richardson
Head of Department,	Ping Yang

August 2013

Major Subject: Atmospheric Sciences

ABSTRACT

The Madden-Julian Oscillation (MJO), a tropical phenomenon that exists on the time scale of 30-90 days, commonly initiates over the Indian Ocean and slowly propagates into the western Pacific as a series of convective events, which have time scales on the order of hours or days. These events and the overall MJO convective envelope may interact with convectively coupled waves such as Kelvin waves that propagate more rapidly eastward with time scales of 3-5 days. Radar and sounding data collected during the DYNAMO/AMIE/CINDY2011 field campaign from October 2011 to February 2012 in the central Indian Ocean are used to study the interaction between Kelvin waves and the MJO in terms of atmospheric and cloud properties. The focus is on characterizing the precipitation characteristics, convective cloud spectrum, and atmospheric profiles of Kelvin waves during the active and suppressed phases of the MJO to gain insight on MJO initiation.

Characteristics of waves identified using different satellite thresholds and filtering methods are compared. Composites of the radar and sounding observations are calculated for a total of ten Kelvin waves and three MJO events that occurred during the field campaign. Analyzed radar products include convective-stratiform classification of rain rate, rain area, and echo-top heights, as well as cloud boundaries. Sounding data includes profiles of wind speed and direction and relative humidity.

Kelvin waves that occur during the suppressed MJO are convectively weaker than Kelvin waves during the active MJO, but display previously documented structure of low-level convergence and a moist atmosphere prior to the wave passage. During the active MJO, Kelvin waves have stronger convective and stratiform rain, and the entire event is longer, suggesting a slower moving wave. The Kelvin wave vertical structure

is somewhat overwhelmed by the convective envelope associated with the MJO. When the MJO is developing, the Kelvin wave displays a moisture-rich environment after the passage, providing deep tropospheric moisture that is postulated to be important for the onset of the MJO.

The convective cloud population prior to MJO initiation shows increased moisture and a population of low- to mid-level clouds. The moisture precedes shallow convection, which develops into the deep convection of the MJO, supporting the discharge-recharge theory of MJO initiation. Additionally, enhanced moisture after the passage of the pre-MJO Kelvin wave could also support the frictional Kelvin-Rossby wave-CISK theory of MJO initiation. With a better understanding of the interaction between the initiation of the MJO and Kelvin waves, the relationships between the environment and the onset of the convection of the MJO can be improved.

ACKNOWLEDGMENTS

First and foremost, I would like to thank my advisors, Dr. Courtney Schumacher and Dr. Anita Rapp, for taking me on as a graduate student. The research opportunity that they provided has given me incredible experiences and knowledge both in the field and in front of a computer. The various conferences and workshops that I have attended and presented at have been educational and rewarding experiences. Thank you for guiding me through the challenges and successes of graduate school and research.

Thanks are due to Dr. Matthew Wheeler and Dr. Carl Schreck for providing their filtering data and for being so kind and helpful through our email correspondence. Their data was an integral part of this thesis. I would also like to thank Dr. Mary Jo Richardson for agreeing to be on my committee and discussing my research with me.

Finally, I would like to thank the members of the A-Team for their help. The A-Team provided a comfortable and stress-free environment to work in and to develop my coding and researching skills. Additionally, I would like to thank Brooke Sutphin for her motivation, and for taking the time to edit my thesis while working on her own. Lastly, thanks to my friends and family in Texas, Florida, New Jersey, New York, and Delaware. It was your support and encouragement that has inspired me to pursue science and complete this journey.

NOMENCLATURE

AMIE	ARM Madden-Julian Oscillation Investigation Experiment
ARM	Atmospheric Radiation Measurement
CINDY2011	Cooperative Indian Ocean Experiment on Intraseasonal Variability in the Year 2011
DYNAMO	Dynamics of the Madden Julian Oscillation
KAZR	Ka ARM Zenith Radar
RH	Relative Humidity
SMART-R	Shared Mobile Atmospheric Research and Teaching Radar
U-Wind/Zonal Wind	East -West component of wind

TABLE OF CONTENTS

LIST OF FIGURES

FIGURE Page

LIST OF TABLES

TABLE Page

1. INTRODUCTION

The Madden-Julian Oscillation (MJO; Madden and Julian, 1972, 1994) is a large-scale tropical convective event that initiates in the Indian Ocean and propagates eastward into the western Pacific Ocean. The dynamics behind its onset are unclear, although there are many theories. In this same tropical region, convectively coupled Kelvin waves frequently occur (Gill, 1980; Wheeler and Kiladis, 1999; Straub and Kiladis, 2002; Masunaga, 2007). Kelvin waves are fast, eastward moving, equatorially trapped atmospheric waves that can be associated with convective events. Since MJO initiation and Kelvin waves both occur in the tropical Indian Ocean, recognizing their convective interactions is potentially important in characterizing and understanding MJO onset.

The Dynamics of the Madden-Julian Oscillation (DYNAMO), the Atmospheric Radiation Measurement (ARM) Madden-Julian Oscillation Investigation Experiment (AMIE), and the Cooperative Indian Ocean Experiment on Intraseasonal Variability in the Year 2011 (CINDY2011) were international field experiments that took place in the Indian Ocean from October 2011 to February 2012. The goal of these campaigns was to collect consistent observations of MJO onset to better understand its initiation. Texas A&M University deployed a C-band, Doppler radar called the Shared Mobile Atmospheric Research and Teaching Radar (SMART-R), which observed precipitating clouds on Addu Atoll, Maldives. At another site on Addu Atoll, the United States Department of Energy (DOE) launched eight soundings per day to observe the vertical profiles of the atmosphere. A vertically pointing cloud radar called the Ka ARM Zenith Radar (KAZR) was also located at this site to observe non precipitating clouds over Addu Atoll.

Data from SMART-R, KAZR, and the soundings collected during the field campaign are used in this thesis to observe and analyze the precipitation and environmental properties of Kelvin waves during the active and suppressed phases of the MJO. Chapter 2 is a literature review of MJO and Kelvin waves that includes background on MJO initiation theories, past field campaigns, and event identification using wave filters. Chapter 3 provides a description of the data products used. Three wave filters are analyzed and compared to identify the strongest events during the field campaign in Chapter 4. Next, the procedures used to analyze the radar and sounding data are explained in Chapter 5. Finally, Chapters 6 and 7 provide results and analysis to show the relationship between Kelvin waves and MJO initiation in the Indian Ocean and overall conclusions are made, leading to the summary of this research in Chapter 8.

2. LITERATURE REVIEW

2.1 The Madden Julian Oscillation

The MJO (Madden and Julian, 1972, 1994) is a large-scale, convective event that initiates in the Indian Ocean and propagates eastward into the Western Pacific Ocean. An MJO event typically occurs in a period of 30 to 90 days and is associated with deep convection and intense, heavy convective rainfall that develops into large amounts of less intense stratiform rain (Zhang, 2005).

The deep convection and dynamics of the MJO not only affects the tropical Indian Ocean and western Pacific Ocean, but because the MJO is a planetary scale disturbance, studies have shown that its effects also extend to both the tropics and the extratropics (see Zhang, 2005). Within the tropics, the large amplitude of the MJO has arguably the biggest variations besides the seasonal cycle. Studies have shown that the MJO can be linked to tropical cyclone activity in both the Pacific Ocean basin and the Atlantic Ocean basin Barrett and Leslie (2009). The active MJO provides a favorable environment for tropical cyclogenesis and more intense events while the suppressed MJO provides an unfavorable environment for tropical cyclones to exist. Additionally, strong MJO events switch from south of the equator to north of the equator as the seasonal cycle changes from austral summer to boreal summer, and this shift affects the Australian monsoon in austral summer and the Asian monsoon in boreal summer (see Zhang, 2005 and references therein). The MJO's reach also extends to the extratropics and can work with the polar jet to bring heavy rainfall and flooding to the west coast of the United States. These Pineapple Express events occur when the MJO propagates into the western Pacific Ocean and its associated moisture extends into the northeast Pacific, across Hawaii.

The polar jet stream splits forming a mid latitude trough, which carries the MJO moisture to the west coast of the US and casues several days of heavy rain and flooding (Bond and Vecchi, 2003).

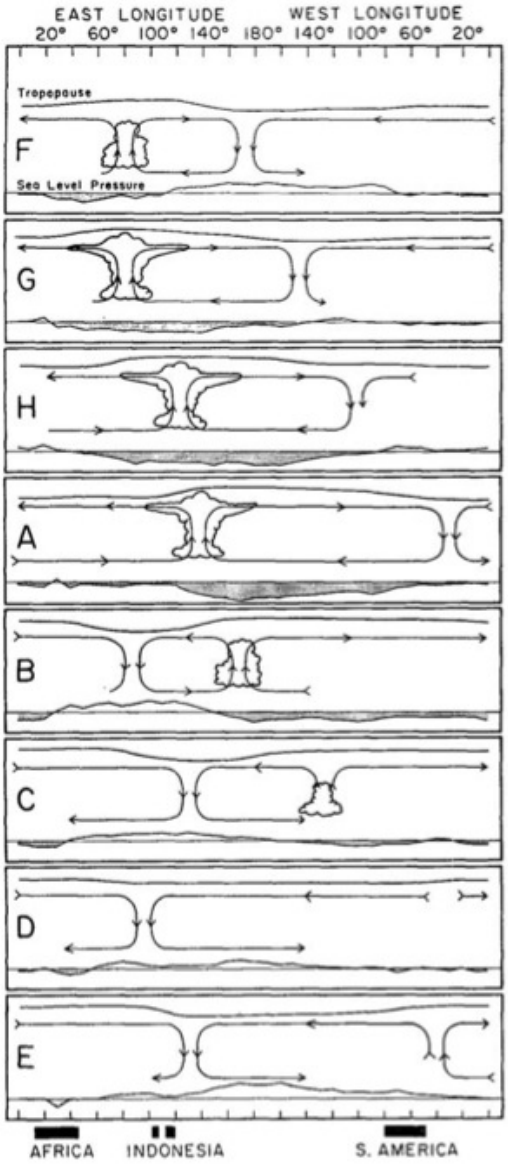

Figure 2.1: Original phase schematic of the MJO. Convection begins over the Indian Ocean and propagates eastward until is dissipates in the Pacific Ocean. Lower-level easterlies exist out in front of the MJO with westerlies behind it. Winds converge at the convective center and diverge at upper levels. From Madden and Julian (1972).

The deep convection during an MJO event can be observed from remotely retrieved outgoing longwave radiation (OLR) measurements (Wheeler and Kiladis, 1999). These measurements are used as a proxy for convection where the lower OLR values are considered deeper convection, i.e. colder cloud tops. Upper and lower zonal wind signatures are another significant feature of MJO events. In the lower troposphere and near the surface, strong westerly winds are present to the west of the convective MJO center. To the east of the convective center there are easterly winds in the lower troposphere, consistent with low-level convergence at the convective center. At upper levels, winds to the west of the MJO center are easterly, and winds to the east of the center are westerly (Zhang, 2005). This overturning circulation is illustrated in Figure 2.1 (from Madden and Julian, 1972).

Also demonstrated in Figure 2.1 are the eight phases of the MJO, labeled A through F. This is the original phase diagram used by Madden and Julian (1972), which centers the MJO over Canton Island in the Central Pacific Ocean (convection location in phase A; 3°S, 172°W), but it has since evolved. The phase indices typically used today are based on the Wheeler and Hendon (2004) index and begin with negative OLR anomalies over Africa and the Western Indian Ocean (Phase 1), which move eastward over the Indian Ocean (Phase 2 and 3), to the Maritime Continent (Phase 4 and 5), to the Western Pacific (Phase 6 and 7) and end where it originated in the western hemisphere and Africa (Phase 8) (Figure 2.2; from Wheeler and Hendon, 2004). The MJO is considered to be in an active phase when deep convection and precipitation occurs. Regions around the deep convection are considered inactive or suppressed phases, and are associated with low precipitation and decreased cloud cover. The Wheeler and Hendon (2004) phase index is determined using empirical orthogonal functions (EOFs) of OLR, 850 hPa zonal winds and 200 hPa zonal winds and provides a consistent index of the daily location of the MJO.

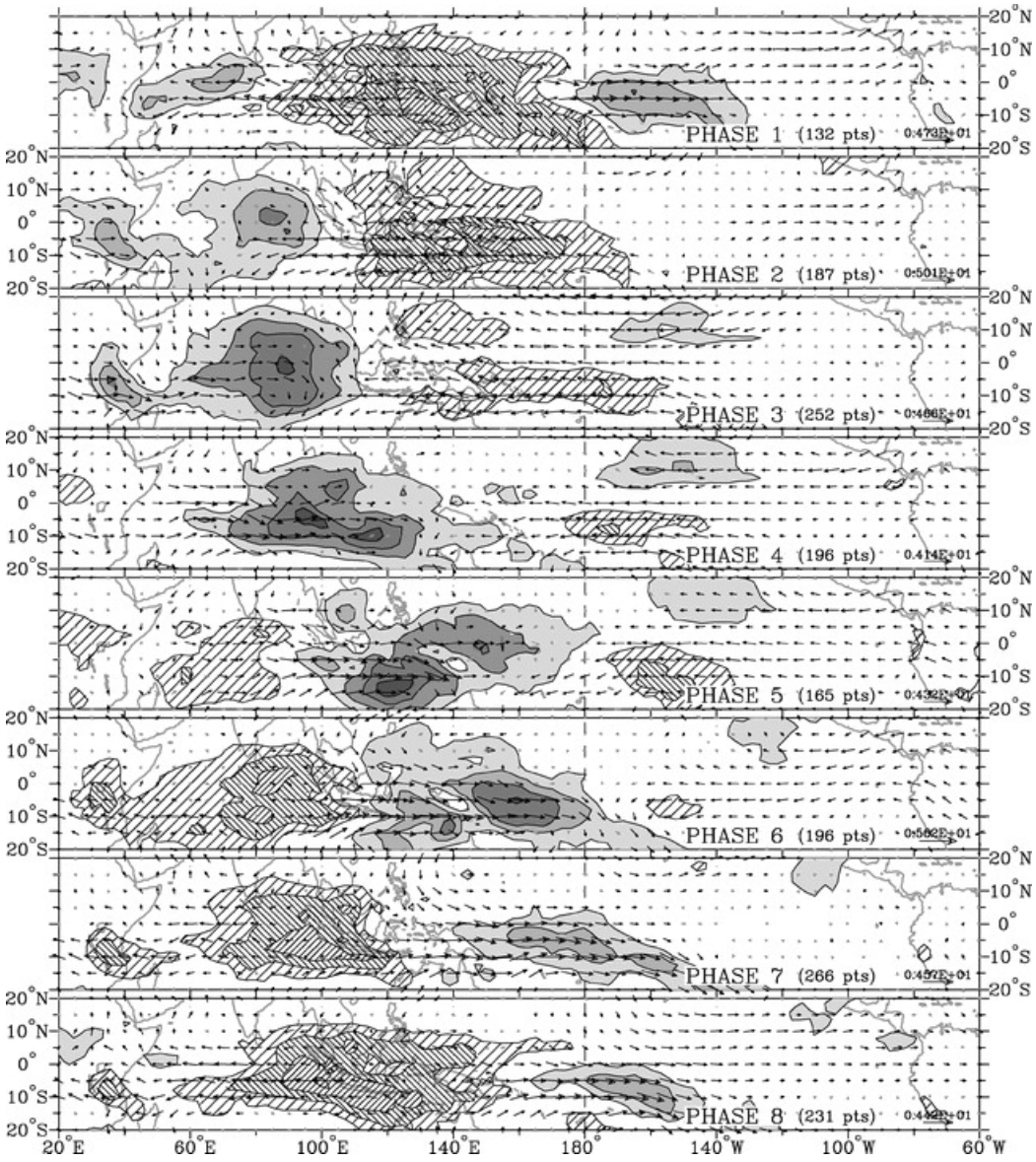

Figure 2.2: New MJO phases. Shaded (hatched) contours are negative (positive) OLR anomalies. Arrows denote magnitude and direction of 850 hPa wind anomalies. MJO initiation begins over Africa in phase 1 and moves eastward to the Pacific Ocean by phase 8. From Wheeler and Hendon (2004).

The cloud population varies throughout the phases of the MJO. Prior to MJO initiation, the cloud spectrum is mostly dominated by shallow, non-precipitating clouds, which serve to increase lower tropospheric moisture (e.g., Blade and Hartmann, 1993). As the shallow clouds deepen and begin precipitating, the moistening

from shallow cloud detrainment and moisture convergence due to low-level diabatic heating helps to precondition the atmosphere for deep convection to occur (Blade and Hartmann, 1993; Lau and Wu, 2010). Hence, the distribution of cloud types and their properties will determine how well the clouds supply moisture and heat to the lower troposphere. In the latter stages of the MJO, the deep convective clouds organize into larger systems with widespread stratiform rain regions, which elevates the heating profile (Houze, 2004; Lau and Wu, 2010).

2.2 Kelvin Waves

Similar to the MJO, the convectively coupled Kelvin wave is an eastward moving tropical convective event (Gill, 1980; Wheeler and Kiladis, 1999; Straub and Kiladis, 2002). Kelvin waves travel at a much faster speed than the MJO, moving at approximately 17 ms^{-1}, while the MJO moves at about 5 ms^{-1} (Straub and Kiladis, 2003). These disturbances are much more frequent than the MJO and are present at all longitudes in the tropics, though they are most prevalent during the boreal summer in the central Pacific and Indian Ocean (Masunaga, 2007). Like the MJO, the location of the Kelvin wave can be identified using a combination of OLR and zonal winds. Low-level westerly anomalies are present within and to the west of the region of lowest OLR, while low-level easterly anomalies occur to the east. Figure 2.3 illustrates this in a schematic of the Kelvin wave by Straub and Kiladis (2003). The structure of humidity and temperature in the Kelvin wave is also illustrated in Figure 2.3. To the east of the Kelvin wave warm, moist anomalies exist at lower levels and continue up to 300 hPa within the convective envelope. To the west of the Kelvin wave cool, dry anomalies exist at lower levels.

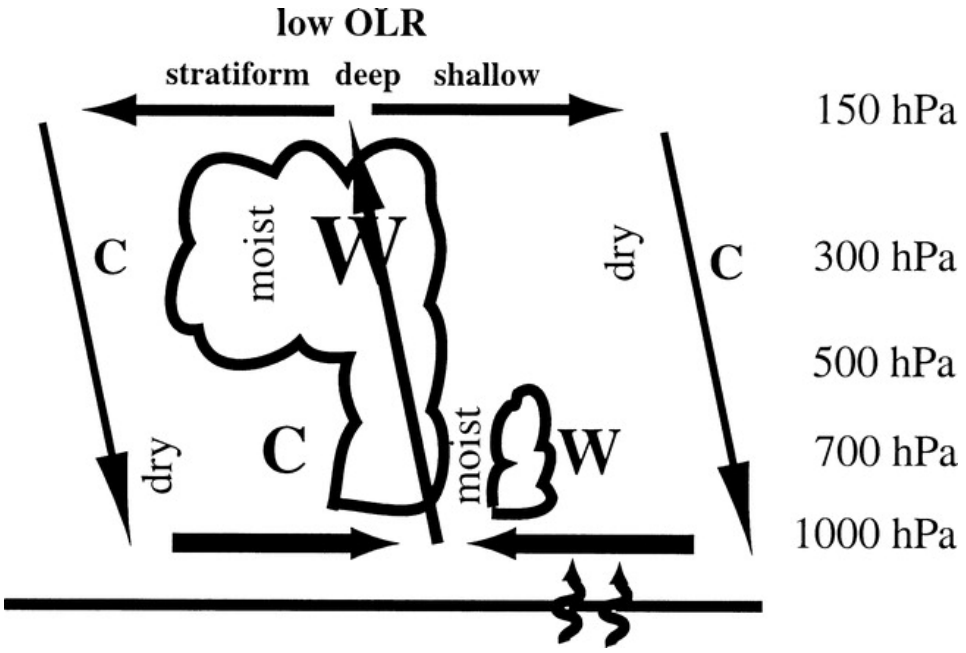

Figure 2.3: Schematic of the Kelvin wave. C (W) signifies cold (warm) anomalies and arrow and text size represent strength of the anomalies. From Straub and Kiladis (2003).

Kelvin waves occur near the equator in the Indian Ocean and produce a combination of convective and stratiform rain. A previous case study in the East Pacific showed that stratiform precipitation is responsible for more than 50% of the total rain area during a Kelvin wave (Straub and Kiladis, 2002). In addition, these fast-moving, short-lived waves can exist during periods of both active and suppressed MJO. A study by MacRitchie and Roundy (2012) calculated a 10-year climatology of MJO and Kelvin wave using rainfall data from the Tropical Rainfall Measuring Mission (TRMM) satellite in the Indian Ocean (5°N to 5°S, 65° to 115°E). They showed that 62% of total rainfall during an active MJO occurred during a Kelvin wave. Furthermore, rain rates were 60% higher when a Kelvin wave is present during an active MJO, and that Kelvin waves were responsible for 46% of the total rainfall area.

Another composite study looked at Kelvin waves during the active and suppressed phases of the MJO in the Indian Ocean (from 5°N to 5°S, at 80°E) using OLR and reanalysis data (Roundy, 2008). This study showed that Kelvin waves move faster during the suppressed MJO than during an active MJO. They also found that waves in both MJO phases showed a similar wind structure to the Straub and Kiladis (2003) schematic (Figure 2.3), where low-level westerlies coincide with convection, although the low-level easterlies of Kelvin waves during the active MJO were much weaker than during the suppressed MJO. Roundy (2008) suggested that during the suppressed MJO, the raining stratiform clouds, or nimbostratus, were deeper and more amplified. However, during active MJO, these clouds were weaker and reduced.

2.3 Theories of MJO Initiation

The mechanisms behind the initiation of the MJO have been attributed to different environmental characteristics such as radiation, surface evaporation, water vapor, SSTs, and other wave events (see Zhang, 2005 and references therein). There are three main types of theories regarding MJO initiation: stochastic processes, external forcings, and internal forcings. Stochastic processes are random fluctuations in energy such as momentum and heating, which could generate an MJO event (e.g., Majda and Biello, 2004). External forcings are drivers from perturbations in the extratropics, which have been thought to provoke MJO initiation (e.g., Lau and Peng, 1987; Hsu et al., 1990; Lau et al., 1994). These extratropical triggers include Rossby wave forcing, where Rossby wave trains travel into the Indian Ocean and cause a rapid increase in upward motion, which initates MJO convection (Hsu et al., 1990).

Internal forcings are triggers within the tropics that could initiate MJO convection. The wave-CISK (Conditional Instability of the Second Kind) theory explains

a positive feedback between convection and large-scale equatorial waves (Yamasaki, 1969; Hayashi, 1970; Lindzen, 1974; Seo and Kim, 2003). In this theory, a frictional convergence of moisture occurs at the leading edge of deep convection during the developing stage of the MJO. A second area of surface convergence also exists to the east of the convection center that pulls the convection eastward. Boundary-layer moisture convergence is provided by globally circling Kelvin waves from the previous active MJO cycle and by Rossby waves from the suppressed convection regions. Figure 2.4 (from Seo and Kim, 2003) illustrates the Kelvin and Rossby propagation.

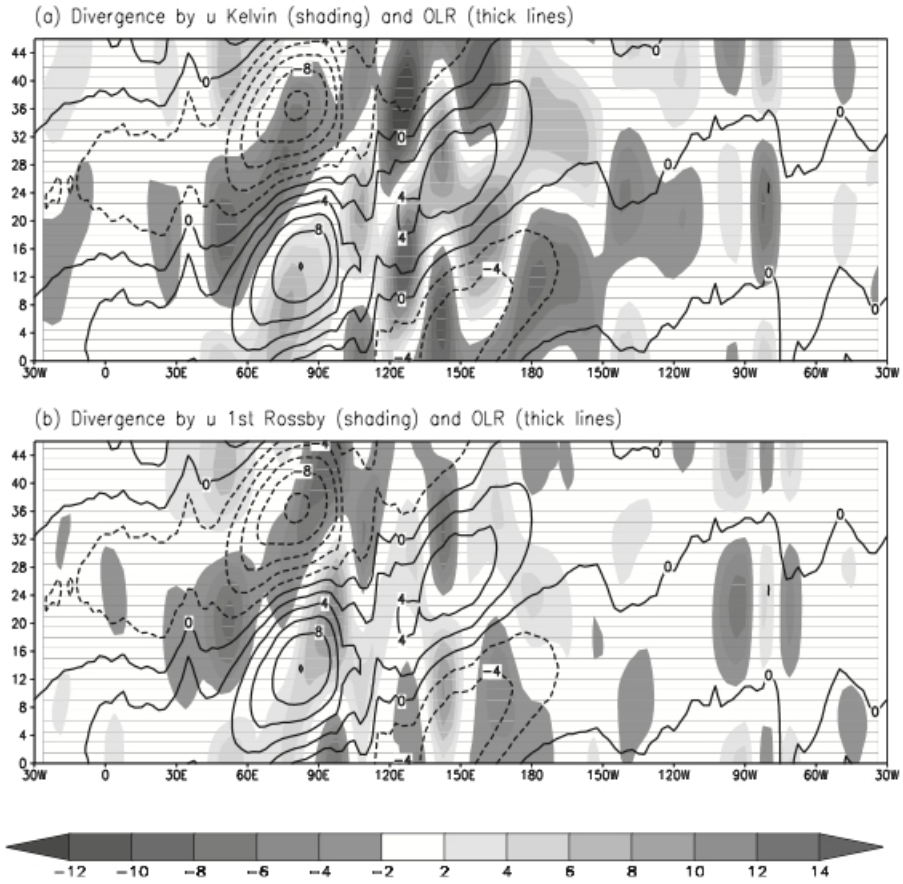

Figure 2.4: Hovmöller plots of zonal convergence by a) Kelvin waves and b) Rossby waves. Dark shading indicates convergence. Dotted lines contour negative OLR anomalies. From Seo and Kim (2003).

The convergence zone is formed around 50°E at 20 days, east of the MJO convection. These waves also work to suppress convection to the west of the MJO event. This theory is formally referred to as the frictional Kelvin-Rossby wave-CISK theory (Seo and Kim, 2003).

An alternate theory of MJO initiation is known as the discharge-recharge hypothesis (Blade and Hartmann, 1993; Kemball-Cook and Weare, 2001) in which both internal and external forcings could cause the MJO. This theory suggests that MJO events are initiated from the combination of mid-troposphere drying and low-level moistening as illustrated in Figure 2.5 (from Kemball-Cook and Weare, 2001). The low-level moistening promotes the formation of shallow convection, which enhances instability and preconditions the atmosphere for deep convection. Once the atmosphere is unstable, an external forcing like extratropical Rossby waves could initiate the next MJO event.

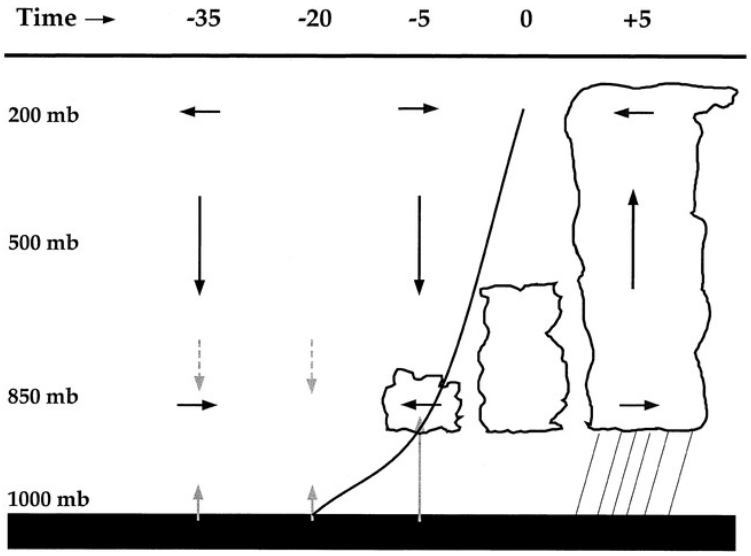

Figure 2.5: Schematic of discharge-recharge MJO initiation theory. Black arrows are wind anomalies. Gray solid arrows are moistening of the boundary layer and gray dashed arrows are drying by entrainment of upper dry air. From Kemball-Cook and Weare (2001).

2.4 Past Field Campaigns

There have been various tropical field campaigns in the past that have observed MJO events and Kelvin waves. The Tropical Ocean-Global Atmosphere Coupled Ocean-Atmosphere Response Experiment (TOGA COARE, Webster and Lukas, 1992) took place from November 1992 to February 1993 in the tropical Western Pacific. Instruments used for observations included moorings, buoys, radars, and soundings. Although TOGA COARE was specifically designed to study the El Niño-Southern Oscillation (ENSO), the observations provided a strong basis for studying the MJO once it propagated into the Pacific Ocean. During this program, two strong MJO events occurred. A study by Yanai et al. (2000) used a combination of the TOGA COARE, reanalysis, and OLR data to study the structure of the MJO. They found that the MJO signal in zonal winds was evident before the deep convection emerged. Once the deep convection formed, the cloud envelope moved eastward with low-level westerlies and upper-level easterlies, along with warm air in the upper troposphere. They suggested that the interaction between the MJO and equatorial waves be investigated to understand their relationships.

A second smaller, but more recent field campaign took place in the Indian Ocean from October to December 2006. This program, called the Mirai Indian Ocean cruise for the Study of the MJO-convection Onset (MISMO; Yoneyama et al., 2008), set out to specifically observe the MJO and its initiation processes. MISMO took observations using radar, soundings, lidar, surface meteorological stations, and ocean measuring instruments. Their findings support the idea that low- and mid-level convection precondition the atmosphere for the deep convection of the MJO. Individual studies have examined the structure of eastward-propagating convective events and compared them with Kelvin waves (e.g., Katsumata et al., 2009; Yamada et al.,

2010), but studies on the interaction of Kelvin waves and the MJO are limited.

2.5 Wave Filtering

The MJO and Kelvin waves are located in space and time using a wavenumber-frequency spectrum analysis, as demonstrated by Wheeler and Kiladis (1999, hereafter WK99). This filtering method uses OLR from all longitudes and tropical band latitudes with satellite-derived deep-layer tropospheric temperatures to identify equatorial waves. These waves are characterized by four parameters: meridional mode number, frequency, planetary zonal wavenumber, and equivalent depth. Meridional mode number is odd for waves that are symmetric and even for waves that are antisymmetric about the equator. Frequency refers to the number of days that the event occurs. Planetary zonal wavenumber is the number of waves around a latitude circle and equivalent depth is a constant that links vertical structure to the shallow water wave equation.

In order to filter waves out of satellite-retrieved OLR, WK99 performed a space-time spectra analysis, which decomposes OLR based on time and longitude into wavenumber and frequency components. OLR power is then calculated by using successive overlapping segments of spectral quantities from the OLR dataset. A series of fast Fourier transforms are performed and the OLR power is averaged, summed by tropical latitudes, and the degrees of freedom are reduced to symmetric and antisymmetric components. Similarly, cross-spectra are calculated using the same method and a different number of overlapping segments. The background spectrum is found by averaging the antisymmetric and symmetric power OLR and smoothing it with a 1-2-1 filter.

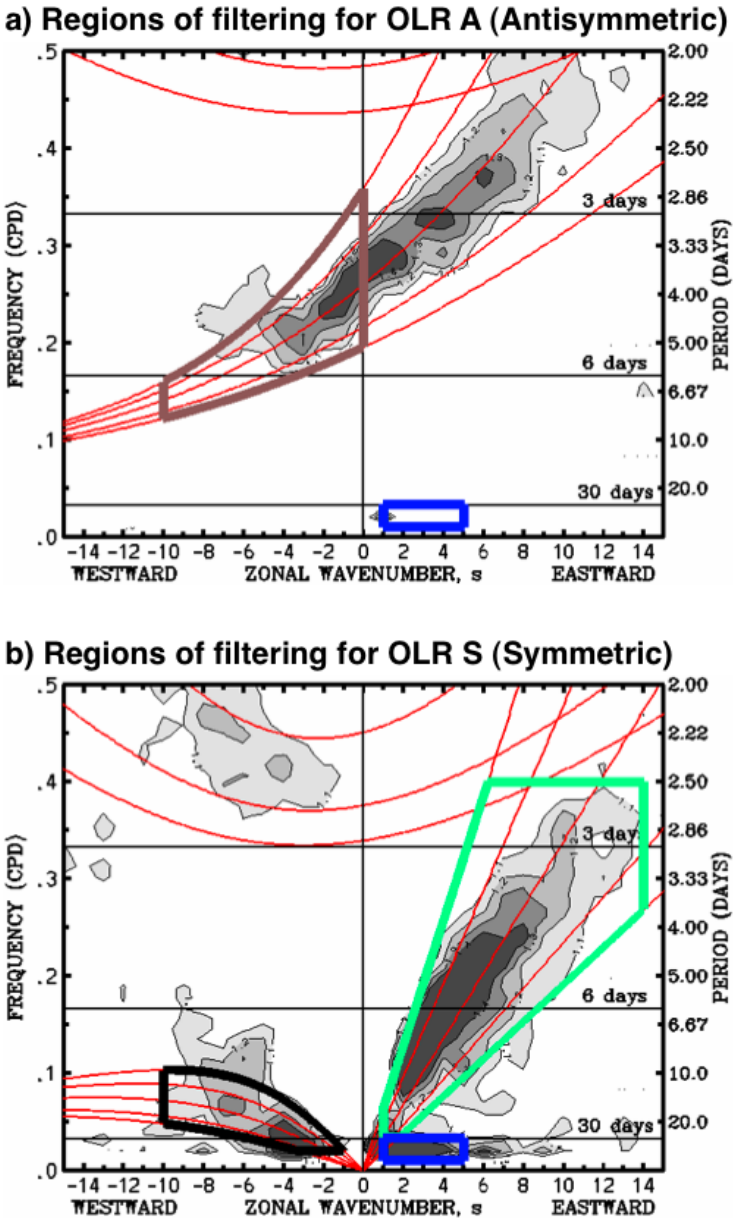

Figure 2.6: Antisymmetric (a) and symmetric (b) wave dispersion curves. MJO (blue outline) is evident in both antisymmetric and symmetric modes, while the Kelvin wave (green outline) is only a symmetric mode. From Wheeler (2013).

The antisymmetric and symmetric power OLR spectra are then divided by the background spectrum to obtain the wave dispersion curves, as shown in Figure 2.6 (from WK99). The wave dispersion curves illustrate the wavenumbers and frequencies that correspond to eastward and westward propagating waves. The MJO (blue outline) has signals in both the antisymmetric and symmetric OLR, and ranges from eastward wavenumbers 1 to 7 and a period from about 30 to 96 days. Kelvin waves (green outline) have only a symmetric OLR signal, with eastward wavenumbers from about 1 to 14 and a period from about 2.5 to 20 days. Once the wavenumbers and frequencies of each wave are determined, the waves can be filtered out from a global OLR dataset. Changing the values of wavenumbers and/or frequency of waves being filtered will alter the number of waves and dates of waves identified, thus providing numerous distributions of waves using the same initial data. Since there are no universal wavenumber-frequency values for equatorial waves, taking a global OLR dataset, extracting specific waves during a specific time period, and analyzing the characteristics of those waves is complex and variable and is addressed in Chapter 4.

3. DYNAMO/AMIE/CINDY2011 DATA

3.1 Field Campaign

The DYNAMO/AMIE/CINDY2011 experiments were recent field campaigns with the goal of understanding the dynamics of the MJO. The multi-nation project focused on collecting data to understand the initiation of the MJO in the equatorial Indian Ocean, and its evolution eastward into the western Pacific Ocean. From October 2, 2011 to February 9, 2012, continuous radar observations and soundings were made in the equatorial Indian Ocean and western Pacific Ocean. Figure 3.1 illustrates the atmospheric sounding array, which spans from about 10°N to 10°S and 70°E to 80°E. Within this array, ground, ship, and aircraft radars, along with radiosondes were used to observe MJO initiation. During this time, three clear MJO events occurred along with various Kelvin waves (Gottschalck et al., 2013). The data products used for this study were located on Addu Atoll, Maldives (0.6°S, 73°E), as shown by the star in Figure 3.1. Observations at this location are positioned in phase 2 and 3 of the MJO (see Figure 2.2), during the initiation.

3.2 SMART-R

SMART-R is a truck-mounted C-band Doppler radar that was deployed by Texas A&M University on Addu Atoll, Maldives (Figure 3.2). Radar is an active sensor, which radiates a pulse of electromagnetic radiation at a specific wavelength. Once the signal makes contact with an object (i.e., precipitation, cloud particles, etc.) in its path, the radiation is scattered back towards the radar and is collected by its receiver. Reflectivity, or echo, is dependent on the size distribution of the objects detected in a given sampled volume and is proportional to the sixth power of the

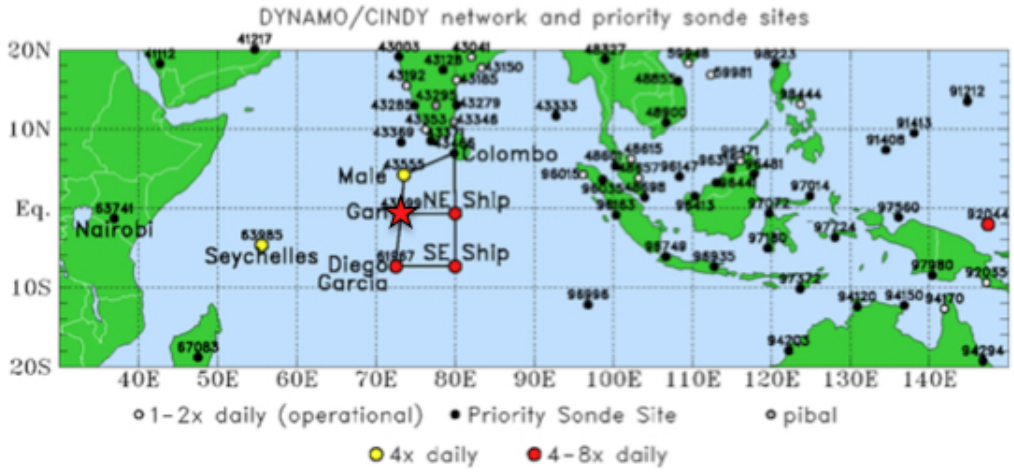

Figure 3.1: Field observation network of DYNAMO/CINDY2011/AMIE. The red star denotes Gan Island, where SMART-R, KAZR, and 3-hourly soundings were located. From the DYNAMO Operations Plan.

particle's diameter. Radars are particularly sensitive to the size of the hydrometeors versus number. High values of reflectivity (i.e., $>$ 40 dBz) indicate an intense storm. Additionally, the transmitted wavelength will determine the sensitivity of the radar. Longer (i.e., cm) wavelengths can detect larger, raindrop-sized particles, and have better transmissivity through the atmosphere. SMART-R is a 5-cm wavelength radar, which is ideal for observing precipitation, but misses non-precipitating and lightly precipitating clouds. In addition, SMART-R is Doppler-capable and can measure the radial velocity of particles towards or away from the radar within the sample volume. Once the transmitted pulse of energy makes contact with a moving particle (i.e., rain drop or cloud particle) the reflected frequency is shifted higher or lower depending on the movement of the particle. The velocity of the particles can then be calculated by comparing the original transmitted frequency and the new returned frequency.

SMART-R ran on a 10-min scan cycle that included three range-height indicator scans (RHI) at various azimuths out to 100 km, a low-level surveillance scan out to

300 km, and two volume scans wit 13 elevation angles each out to 150 km from the radar. Due to beam blockage at low levels from trees in the west, radar products have been analyzed to only include the 180 degree sector between 338° and 158°, which limits the data products to a smaller area. These analyzed radar products include echo-top heights, rain rate, rain area, and convective-stratiform classification. Echo-top heights are a measure of the vertical structure of the rain event, which serves to detect the height of the precipitation echoes based on reflectivity thresholds. Rain rates are calculated using a reflectivity to rain rate relationship, also known as a Z-R relationship. The Z-R relationship used to calculate rain rate from SMART-R is the same one used for the MISMO campaign (see Fliegel, 2012 for more information). Rain area is the fraction of the echoes' coverage of the radar area. Rain rates and

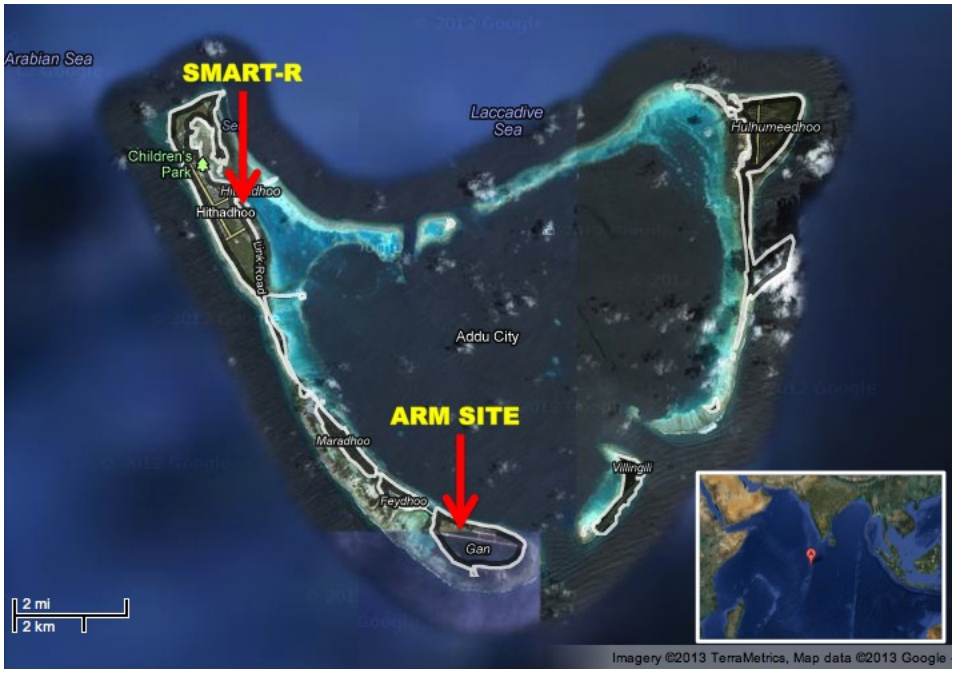

Figure 3.2: Map of field observations on Gan Island, Maldives (0.6°S, 73°E). Red arrows denote the location of SMART-R and the ARM site where the KAZR and soundings were located. (Base map available from maps.google.com)

area are separated into convective and stratiform rain by classifying the reflectivity using a modified algorithm based on Steiner et al. (1995). In the tropics, convective rain is most common and occurs in intense storms with higher reflectivity (e.g., 40 dBz). Stratiform rain typically develops after a convective event as rain covering a large area and has a lower value of reflectivity (e.g., 10-20 dBz). A reflectivity threshold along with a texture test to assess peakedness thus separates the SMART-R rain rates. The modification to the Steiner et al. algorithm uses echo-top information to reclassify shallow, isolated cells as convective (Fliegel, 2012).

3.3 KAZR

The vertically pointing KAZR was located at the ARM site on Addu Atoll (Figure 3.2). Like SMART-R, KAZR is an active sensor that remotely detects cloud particles in the atmosphere. KAZR is more sensitive than SMART-R because it radiates at an 8.6 mm-wavelength, allowing it to detect smaller cloud-sized droplets. However, this shorter wavelength is attenuated more quickly when it travels through larger precipitation-sized particles. In addition, KAZR is a vertically pointing Doppler radar, meaning it only observes the atmosphere directly above it, as opposed to a scanning radar like SMART-R, which moves horizontally and vertically. This limits the observations of KAZR such that it will only record clouds that move directly over the radar, and hence can miss clouds observed by SMART-R.

KAZR began radiating on October 8, 2011 and continued through February 8, 2012, recording observations at 4-second intervals. The radar has a resolution of about 30 m from the ground to almost 20 km in altitude. Due to the sensitivity of the radar, cloud base height and cloud top height measurements are used in this thesis to obtain the cloud evolution of convective events. The data product used is

the KAZR Active Remote Sensing of Clouds (ARSCL) Value Added Product (VAP), which combines observations from other instruments with the KAZR cloud observations for a more accurate measure of cloud boundaries. The other instrument used for the cloud boundary product is the mircopulse lidar (MPL), also located at the ARM site. Similar to radar, the MPL sends a pulse of energy through the atmosphere to determine the height of cloud bases and tops. The MPL can detect optically thin clouds, but it gets attenuated quickly through precipitation. The combination of the KAZR observations with observations from the MPL improves the measurements of cloud boundaries up to ten levels of clouds.

3.4 Soundings

Atmospheric soundings were deployed at the six locations in the sounding array (Figure 3.1) and launched up to eight times per day. Meteorological radiosondes attached to a weather balloon were released into the atmosphere and recorded atmospheric data every few seconds. Soundings from DOE's second ARM mobile facility (AMF2) site on Gan Island are used in this study (Figure 3.2). These soundings provide profiles of wind speed and direction, temperature, relative humidity, and pressure.

4. EVENT IDENTIFICATION

4.1 Wave Filters

To identify specific wave events from October 2, 2011 to February 9, 2012, three wavenumber-frequency filters are used. These include the original Wheeler and Kiladis (1999) filter, a similar filter used by Carl Schreck (Schreck, 2013), and the DYNAMO-specific filter developed by a group of DYNAMO scientists (Gottschalck et al., 2013). Each filter obtains the wavenumber-frequency regions the same way as WK99, but the actual ranges of wavenumber and frequency vary between the filters, as displayed in Table 4.1. Compared to the Wheeler filter, the Schreck filter is more liberal with MJO filtering in both frequency and wavenumber, but slightly more conservative with Kelvin filtering in frequency. The DYNAMO method is much more generous with MJO filtering in frequency and wavenumber, but also more conservative with Kelvin filtering in frequency than the Wheeler filter.

Table 4.1: Wavenumber and frequency differences in three filters used to identify wave events during DYNAMO.

Filter:	Wheeler	Schreck	Dynamo
MJO			
Wavenumber:	1-5 eastward	0-9 eastward	0-9 eastward
Frequency:	30-96 days	30-100 days	20-100 days
Kelvin Wave			
Wavenumber:	1-14 eastward	1-14 eastward	1-14 eastward
Frequency:	2.5-30 days	2.5-17 days	2.5-20 days

Once the global OLR anomalies are filtered to identify wave events, the filtered data must be averaged by latitude to view the zonal propagation of the waves, which is typically displayed in a Hovmöller plot. Figure 4.1 illustrates interpolated satellite-retrieved OLR averaged from 10°S to 10°N. The Advanced Very High Resolution Radiometer (AVHRR) onboard the National Oceanic and Atmospheric Administration's (NOAA) polar-orbiting satellites collects the OLR data which is provided by the National Center for Environmental Prediction (NCEP). The eastward propagation of the three MJO events (at the end of October, November, and December) is evident where the OLR minimums are located (blue shading). The wider the latitude domain that is averaged, the less variability is preserved. In addition, wider bands decrease the strength of filtered events by washing out the OLR minima. Hence, the latitude domain and wave threshold (OLR minimum) will further vary the waves that are identified. Because this thesis is focused on the precipitation and atmospheric characteristics of these wave events, onset dates and wave passage dates are extremely important when using radar and sounding observations at Gan Island.

4.2 Filtered MJO Events

The filtered MJO events are displayed in Figure 4.2 and include variations based on latitude domain averaging choices. All three filters identify the first two MJO events that occurred during the field campaign at all latitude domains. As the latitude domains widen and the threshold remains at -10 Wm^{-2}, the filtered MJO events become smaller. The DYNAMO filter is the only one of the three that identifies the December event as an MJO, due to its wide range in frequency. In addition, all three filters identify an MJO event that occurred in January. However, there was no rainfall near Addu Atoll during this time. The negative OLR anomalies associated

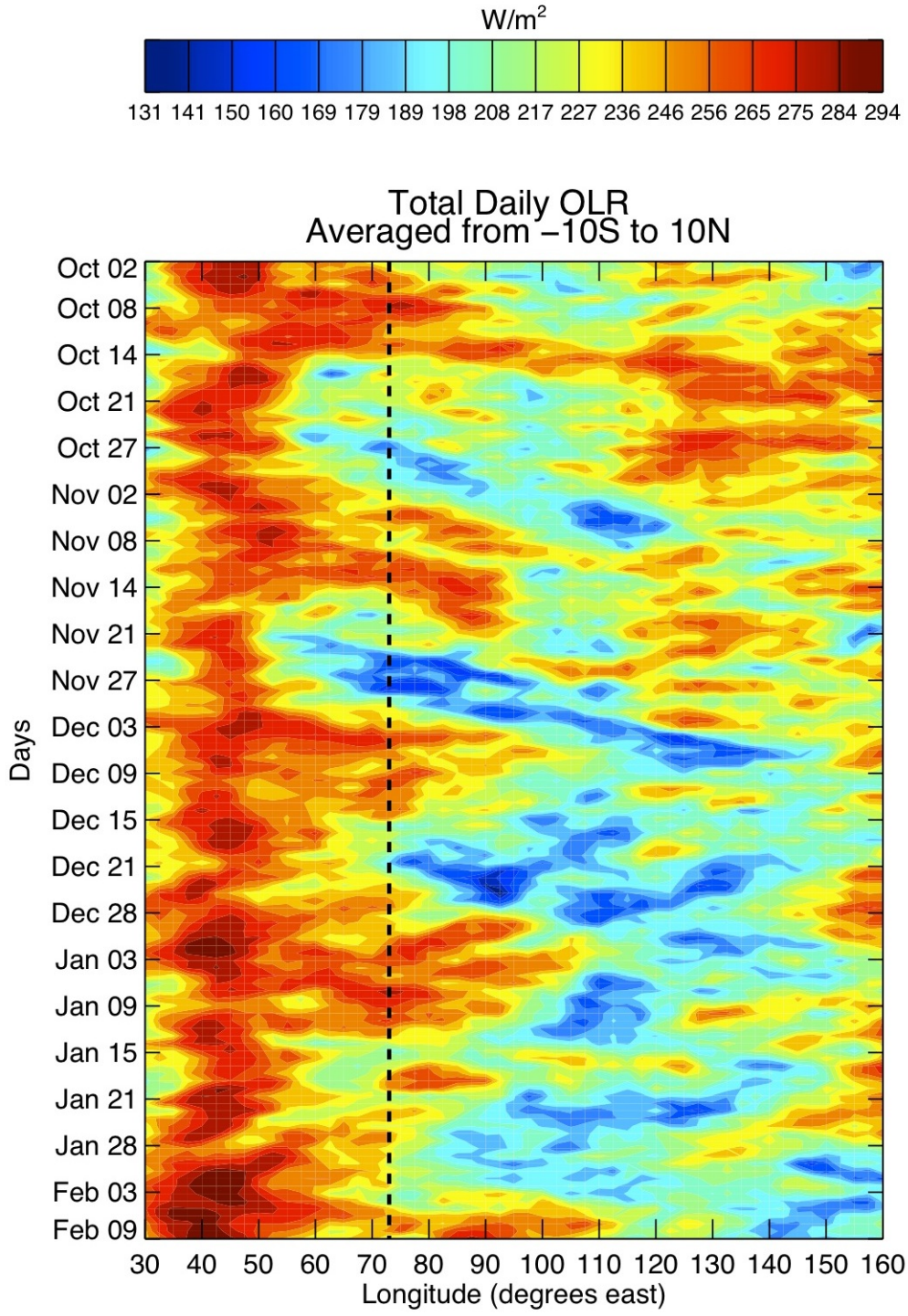

Figure 4.1: Total daily OLR averaged from 10°S to 10°N. Lower OLR values are areas of deep convection. The dotted line locates Gan Island.

with this event are located south of the equator, away from the equatorial Addu Atoll location. MJO onset date and duration at Gan Island varies between the three filters. In Figure 4.2, the dotted line is the location of Gan Island. Each of the first two MJOs begin and end on different days based on filter. For the purpose of this thesis, the three MJO events identified by the DYNAMO filter will be used for analysis for consistency with other studies using the DYNAMO/AMIE/CINDY2011 datasets.

4.3 Filtered Kelvin Waves

Kelvin waves identified by the different filters and domain size are plotted in Figure 4.3. More Kelvin events are identified at smaller latitude domains than wider domains at a common threshold. Table 4.2 lists the number of events identified by each filter at the different latitude domains. The Wheeler filter identifies the most Kelvin waves at smaller latitude domains, due to its wider range in frequency. All three filters are in good agreement for the strongest and longest Kelvin wave events. In addition, note the distribution of Kelvin events that occurred during the field campaign. There is a higher density of Kelvin events during the first half of the campaign (during the first two MJO events) than the second half.

4.4 Latitude Domain Comparison

Maintaining an event threshold of -10 Wm^{-2} demonstrates the importance of choosing latitude domains. At smaller domains, longer and more numerous waves are identified, especially in the Kelvin band for all three filters (Figure 4.3). Because this thesis utilizes radar and sounding data at Gan Island, it is important to illustrate the differences in rain statistics that arise from varying latitude domains. Figures 4.4 and 4.5 display bar graphs of average convective and stratiform rainfall from

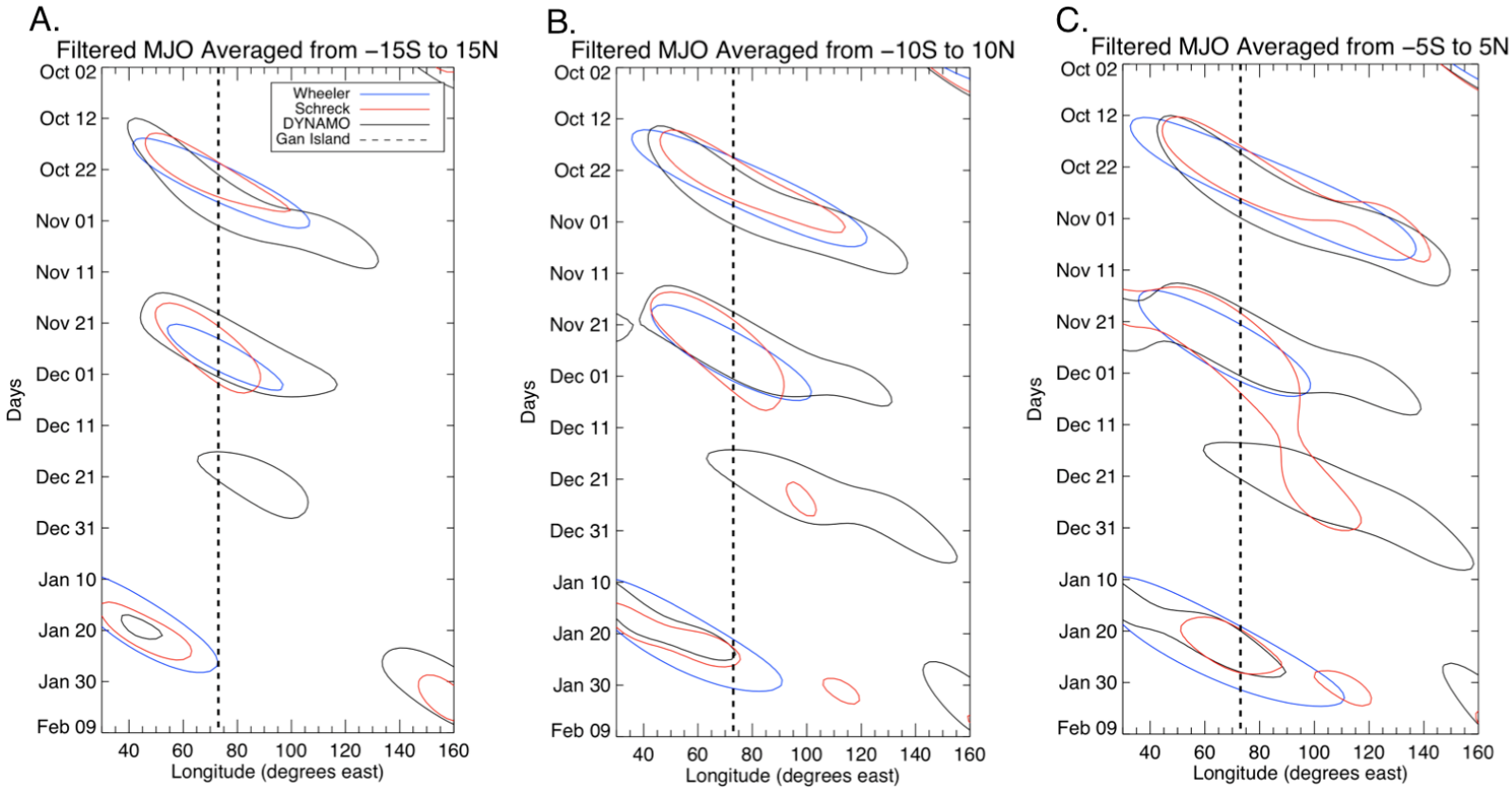

Figure 4.2: MJO filtered OLR at a -10 Wm^{-2} threshold. The Wheeler filter is in blue, Schreck is in red, and DYNAMO is in black. Plotted with three different latitude domains, (a) 15°S to 15°N, (b) 10°S to 10°N, and (c) 5°S to 5°N. The dashed line is the longitude of Gan Island.

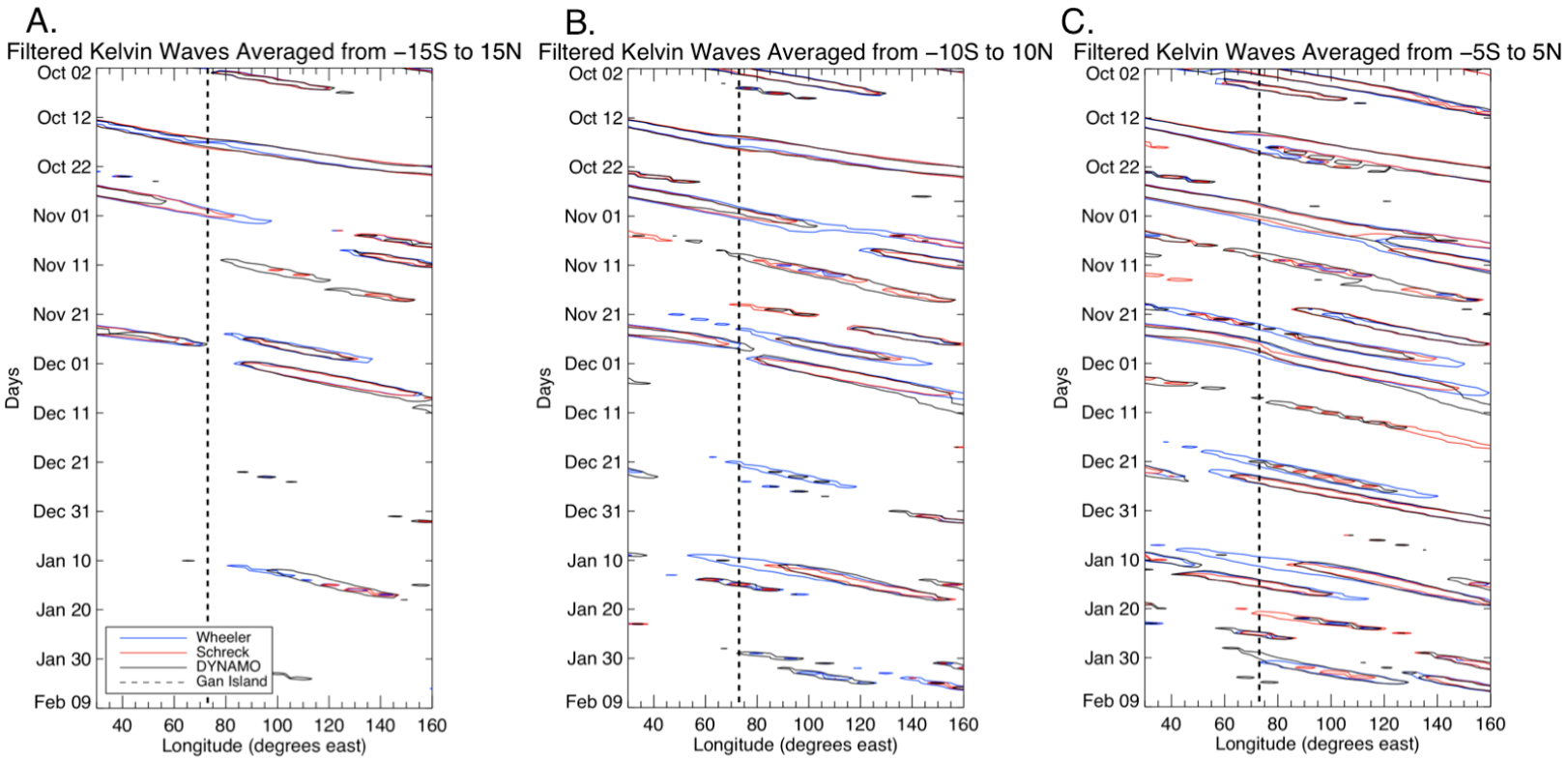

Figure 4.3: Kelvin wave filtered OLR at a -10 Wm^{-2} threshold. The Wheeler filter is in blue, Schreck is in red, and DYNAMO is in black. Plotted with three different latitude domains, (a) 15°S to 15°N, (b) 10°S to 10°N, and (c) 5°S to 5°N. The dashed line is the longitude of Gan Island.

Table 4.2: Number of MJO and Kelvin waves filtered using three filters at three different wave thresholds.

a. Latitude averaged from -5°S to 5°N

Filter:	Wheeler	Schreck	Dynamo	# In Common
Threshold: -10 Wm^{-2}				
# MJO	3	3	4	3
# Kelvin	11	8	10	6
Threshold: -12 Wm^{-2}				
# MJO	3	3	4	3
# Kelvin	10	7	8	5
Threshold: -15 Wm^{-2}				
# MJO	3	2	3	2
# Kelvin	6	4	7	4

b. Latitude averaged from -10°S to 10°N

Filter:	Wheeler	Schreck	Dynamo	# In Common
Threshold: -10 Wm^{-2}				
# MJO	3	2	3	2
# Kelvin	6	5	8	4
Threshold: -12 Wm^{-2}				
# MJO	3	2	3	2
# Kelvin	5	3	3	2
Threshold: -15 Wm^{-2}				
# MJO	1	1	3	0
# Kelvin	1	1	1	1

c. Latitude averaged from -15°S to 15°N

Filter:	Wheeler	Schreck	Dynamo	# In Common
Threshold: -10 Wm^{-2}				
# MJO	2	2	3	2
# Kelvin	2	2	2	1
Threshold: -12 Wm^{-2}				
# MJO	1	2	3	1
# Kelvin	0	1	1	0
Threshold: -15 Wm^{-2}				
# MJO	0	0	2	0
# Kelvin	0	0	0	0

SMART-R during MJO and Kelvin wave events, respectively, separated by filter and latitude domain. Stratiform rain percent is noted at the top of each bar pair. The composite MJO graphs show that MJO events always have more stratiform rain than convective rain, which is consistent with previous studies (e.g., Lin et al., 2004). Stratiform rain percent is generally consistent at the different latitude domain sizes for each filter. However, as the latitude domain gets larger, rain amounts increase because only the largest negative OLR anomalies are filtered (see Figure 4.2).

The composite Kelvin waves display a different trend in stratiform percent when modifying the latitude domain. At smaller domain sizes, there is almost equal stratiform and convective rain and the filters are in good agreement. As the latitude domain is increased, stratiform precipitation decreases relative to convective rain. This is most likely due to fewer identified events introducing higher variability in sampling (see Figure 4.3).

A latitude average of 10°N to 10°S is used for the remainder of this thesis because it encompasses the entire sounding array (Figure 3.1; Gottschalck et al., 2013). Latitudinal averages between 10 and 20 degrees have been used in other studies of equatorial waves over the northern tropical Western Pacific Ocean (e.g., Swann et al., 2006; 0°-15°N) and the northern tropical Eastern Pacific Ocean (e.g., Straub and Kiladis, 2002; 2.5°-15°N). Using this average also accounts for the shift from boreal summer to austral summer.

4.5 Choosing Kelvin Wave Dates

Identifying the specific dates of wave passages is important when using hourly radar and sounding data to analyze the wave features. The filtered data is averaged in longitude to pinpoint the date of passage by finding the local filtered OLR minimum

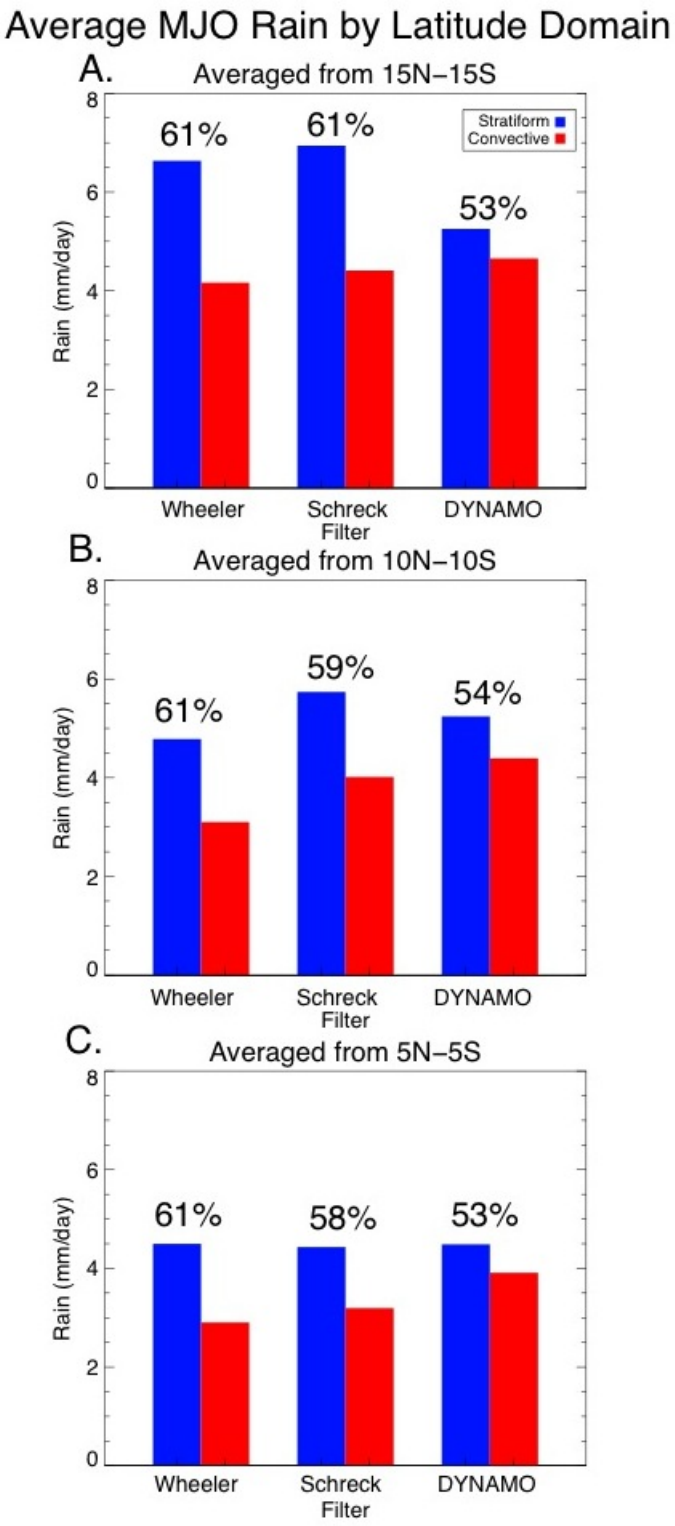

Figure 4.4: MJO convective and stratiform rain amounts by filter and latitude domain. Stratiform rain (blue bar) and convective rain (red bar) totals are plotted. Stratiform rain percent is stated above each stratiform bar.

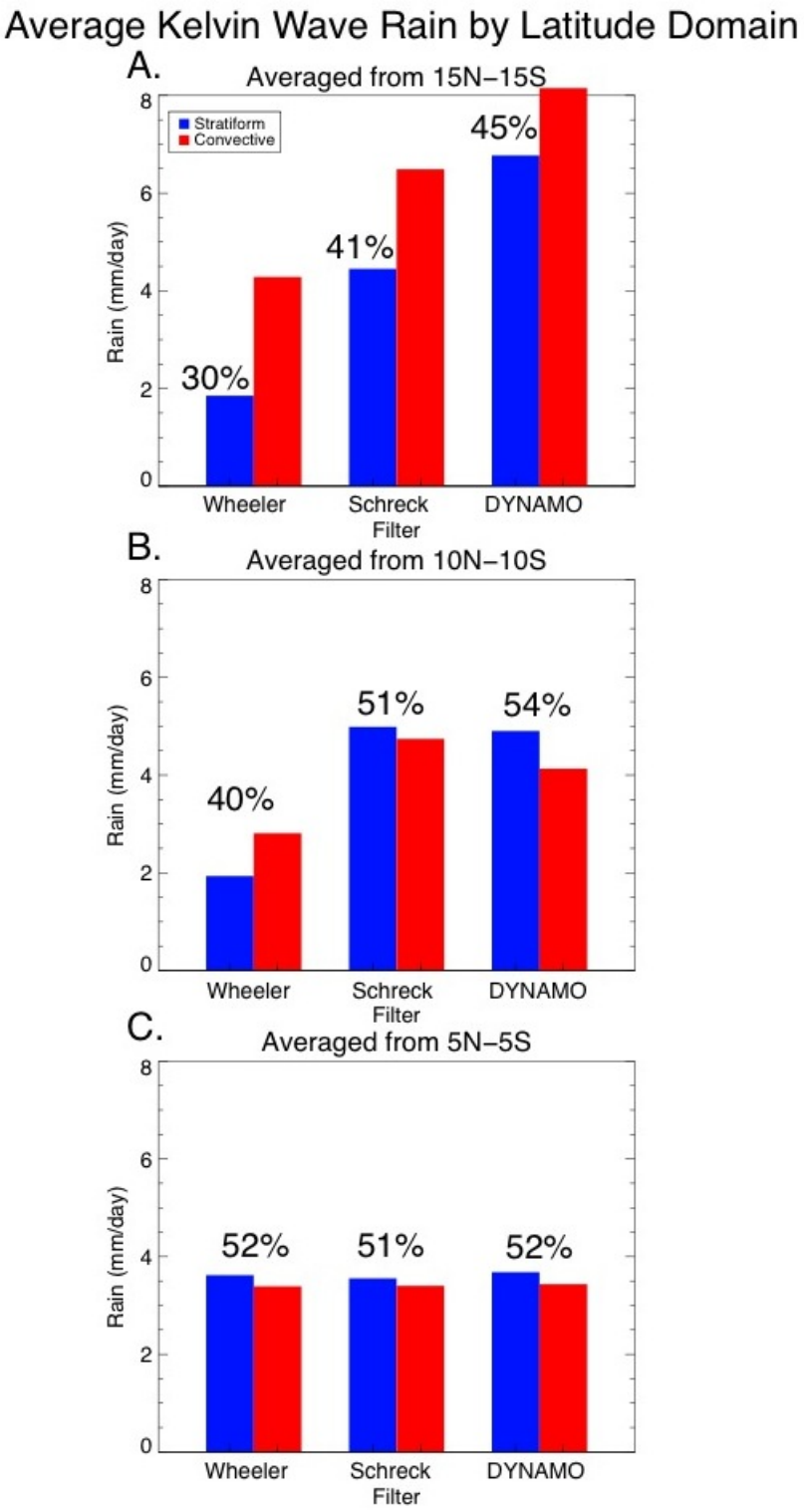

Figure 4.5: Kelvin wave convective and stratiform rain amounts by filter and latitude domain. Stratiform rain (blue bar) and convective rain (red bar) totals are plotted. Stratiform rain percent is stated above each stratiform bar.

anomaly. The longitudinal average used in Gottschalck et al. (2013) is 70°E to 80°E, which encompasses the sounding array (Figure 3.1). However, since this thesis focuses on the precipitation at Gan Island, located at about 73°E, a longitude average from 72.5°E to 75°E is used. This will pinpoint dates of wave passages that should correlate well with convection located within the radar domain.

One way to extract these dates is by calculating the standard deviation of the filtered OLR anomalies and dividing each local OLR minimum by the standard deviation. This provides the distribution of the wave events with a standard deviation of 1.0. Hence the larger negative values are stronger events. Table 4.3 displays the dates and values where at least one of the filters has a date less than or equal to -1.0 standard deviation. Also listed in this table is the daily total convective rainfall and details about the Kelvin wave including when the wave occurred based on MJO events and if it is coupled with convection. By calculating Kelvin wave occurrence using the distribution of standard deviations, dates can easily be compared among the different filters. Notice that each filter has a negative standard deviation for all of the dates listed though the magnitude of the deviation differs by filter. The stronger and more frequent Kelvin waves occur during and around the three MJO events. In addition, the Schreck filter identifies the least number of waves compared to the other two filters, due to its constraint on Kelvin wave frequency (see Table 4.1).

For this thesis, only events that are coupled with convection will be used therefore dates with less than 0.5 mm d^{-1} rainfall will be excluded. The wave dates that are in bold face type are the dates used, which have a standard deviation of greater than -0.6 by all filters. To compare Kelvin waves during the field campaign, three MJO phases are defined: the active phase (when the MJO filtered OLR anomalies are less than or equal to -10 Wm^{-2}), the suppressed phase (when the MJO filtered OLR

Table 4.3: Standard deviations and dates of filtered Kelvin waves. Only dates where at least one filter has a standard deviation of less than or equal to -1.0 are shown. Rain total and details about the dates are listed. Kelvin wave dates used for this thesis are bolded.

Date	Wheeler Filter	Schreck Filter	DYNAMO Filter	Total Convective Rainfall (mm)	Details
Oct 2	-2.1	-1.9	-1.9	1.86	Not enough data
Oct 3	-1.8	-1.7	-1.9	1.42	
Oct 6	**-1.6**	**-1.5**	**-1.7**	**0.69**	Suppressed MJO
Oct 16	-1.2	-1.7	-1.7	8.10	Suppressed MJO
Oct 17	**-1.8**	**-2.4**	**-2.2**	**3.20**	
Oct 18	-1.3	-1.8	-1.5	13.10	
Oct 19	-0.8	-1.2	-1.0	1.99	
Oct 30	-1.1	-0.8	-0.9	2.15	Active MJO1
Oct 31	**-2.3**	**-2.0**	**-1.7**	**7.56**	
Nov 1	-2.1	-1.9	-1.1	2.09	
Nov 9	**-0.7**	**-1.2**	**-1.7**	**2.28**	Suppressed MJO
Nov 10	-0.3	-0.9	-1.0	5.99	
Nov 19	**-1.3**	**-1.7**	**-1.1**	**0.80**	Pre-MJO2
Nov 24	**-1.6**	**-1.0**	**-0.7**	**2.26**	Active MJO2
Nov 27	-1.4	-0.7	-1.7	4.16	Active MJO2
Nov 28	**-1.4**	**-0.8**	**-1.5**	**2.37**	
Nov 29	-1.0	-0.8	-0.7	2.29	
Nov 30	-1.3	-1.2	-0.6	0.47	
Dec 21	-1.4	-0.7	-1.0	8.26	Active MJO3
Dec 22	**-1.3**	**-0.6**	**-1.0**	**7.38**	
Dec 25	**-1.4**	**-1.2**	**-1.0**	**1.85**	Suppressed MJO
Jan 10	-1.7	-1.4	-1.2	0.0	No rain
Jan 11	-1.6	-1.2	-1.4	0.0	
Jan 15	**-1.9**	**-1.9**	**-2.2**	**4.54**	Suppressed MJO
Jan 21	-0.6	-1.1	-0.5	0.03	Little rain
Jan 25	-1.2	-1.2	-1.2	0.06	Little rain
Jan 28	-0.9	-0.7	-1.0	0.04	Little rain
Jan 29	-1.3	-1.1	-1.5	0.31	Little rain
Feb 4	-0.4	-0.6	-1.3	0.12	Little rain

anomalies are greater than or equal to 0 Wm^{-2}), and the pre-MJO phase (when the MJO filtered OLR anomalies are between 0 and -10 Wm^{-2}). The dates that the filtered Kelvin waves occur will determine which MJO phase they are in (see the last column in Table 4.3). From October 2 to February 9, there were four Kelvin waves during an active MJO and five Kelvin waves during a suppressed MJO. November 19, will be examined individually because it was the only event that occurred in the "pre-MJO" phase.

5. COMPOSITE METHODOLOGY

5.1 Calculating Composites

To examine the precipitation and atmospheric properties of the Kelvin wave and MJO, specific cases are composited. The purpose of compositing is to see if there is a relationship between a set of data and a specific variable (i.e., Kelvin waves and relative humidity), which is calculated by averaging conditions based on specific criteria (i.e., hour or day of wave passage). One of strengths of compositing is that the criteria used can be simple or complex, which allows for a range of analyses. It is also beneficial because it allows for any variable to be used (Yarnal, 1993). Although compositing can hide variability or patterns of single events, it can illustrate the overall characteristics of the dataset, which is its main use for this thesis.

Three MJO events occurred during the study period at Addu Atoll. Each event has a date of minimum OLR anomaly, which will be referred to as the peak date, and are listed in Table 5.1. MJO composites are calculated by averaging the three events from 25 days prior to the peak to 20 days after the peak, where the peak date is day 0.

Table 5.1: Peak dates of the three MJO events.

MJO Event	**Peak Date**
MJO1	Oct 28
MJO2	Nov 25
MJO3	Dec 19

Kelvin waves are documented to have their maximum rainfall occur about one day prior to the date of wave passage (Straub and Kiladis, 2002, 2003). The date of wave

passage is based on filtered OLR anomalies, as explained in Chapter 4. Since this thesis focuses on the precipitation characteristics and interactions of wave events, the composites are centered on the maximum convective rainfall during a Kelvin wave passage. This date is located by finding the maximum in the convective-separated hourly rain rate dataset from SMART-R for each of the ten Kelvin waves. The range for locating the convective rain maximum is from 48 hours prior to 24 hours after the date of Kelvin wave passage. Once the hour of maximum convective rainfall is located, each Kelvin wave time series is centered on that hour between the 48 hours of rainfall prior to the maximum and the 48 hours of rainfall after the maximum. Finally, the waves are composited based on their timing during the MJO, i.e., the active, suppressed, or pre-MJO. The dates of the Kelvin waves used for the composites are listed as the bold-face dates in Table 4.3. There are four waves composited during the active MJO and five waves composited during the suppressed MJO. One wave occurred during the pre-MJO period, which is plotted alongside the composites for comparison. It is important to recognize that this study is limited to the small number of cases that occurred during the field campaign.

5.2 SMART-R Composites

SMART-R composites of the active MJO are calculated. For clarity, all hourly SMART-R data are summed for daily accumulation of rainfall or averaged by day for rain area and echo-top heights for these composites. Rain accumulation, rain area, and echo-tops are separated into convective and stratiform types. The retrieved rain accumulation and echo tops are composited to capture the precipitation characteristics of the MJO initiation over Addu Atoll. Additionally, SMART-R Kelvin wave composite time series are calculated for hourly rain rate, rain area, and echo-top

heights, also separated into convective and stratiform types. This will illustrate the precipitation features during Kelvin wave passages.

5.3 KAZR Composites

KAZR cloud-base and cloud-top heights are used to observe the cloud evolution during the MJO events and Kelvin waves during the active, suppressed, and pre-MJO. The composite of MJO cloud counts is calculated by averaging the data into ten-minute intervals and centering them at 0 Z on the peak day, with 25 days prior and 20 days after the peak day. Counts are found by binning the data into 180 m by 3-hour bins for the three MJO events, counting each vertical bin where a cloud is present from the cloud-base height to the cloud-top height. Composites are calculated by dividing the counts by the number of sampled events. Profiles are calculated by summing the cloud counts at each level over a five day period. This cloud count analysis provides an illustration of the evolution of clouds during the passage of MJO events and Kelvin waves over Addu Atoll.

For the Kelvin wave counts, the KAZR data are averaged to one-minute intervals. To find the cloud counts, the waves are first centered on the hour of convective maximum, as for the SMART-R composites, with 48 hours of data before and after the center hour. Then, the data are totaled into 100 m vertical by 10 min bins and separated by occurrence during active and suppressed MJO. These bin sizes are different than for the MJO events because the Kelvin waves have a smaller temporal scale. Composites are then calculated by dividing the counts by the number of sampled events in each phase. Since the KAZR started radiating on October 8, 2011, it missed the first Kelvin wave during the suppressed phase of the MJO. Hence, the suppressed MJO KAZR cloud profile composites include only four Kelvin waves, not

including the October 6th wave. The counts for the single pre-MJO event are found as well. Counts are plotted as cloud population profiles. Profiles are calculated by summing the cloud counts at each level over six separate 12-hour periods throughout the Kelvin waves to observe the temporal evolution of the vertical distribution of clouds.

5.4 Sounding Composites

The soundings on Gan Island were launched eight times per day, or every three hours. For the MJO composite, the soundings are averaged by day so that day 0 corresponds to soundings from the peak day. Composites of the relative humidity are calculated and plotted to examine how the vertical structure of the moisture associated with the MJO evolves after it is initiated in the Indian Ocean. The composite relative humidity is also used to compute lag correlations of rain accumulation with upper (200-600 hPa) and lower (700-960 hPa) tropospheric relative humidity (similar to Sobel et al., 2004, Figure 5.1) using a 1-day lag. The study by Sobel et al. (2004) looked at intense convective events in the tropical central Pacific Ocean and the relationship between moisture from soundings and radar derived rain rate. They found that the lower tropospheric relative humidity precedes the development of convective rain. Then, the upper tropospheric relative humidity follows the development of stratiform rain. The relative humidity and rain rate lag correlations are used to observe the convective and stratiform evolution with relative humidity of the MJO and Kelvin wave events.

Zonal wind anomaly composites are also calculated. The anomalies are computed by averaging the zonal winds at each vertical level for the entire time series. The level averages are then subtracted from each zonal wind value at that level to calculate

the anomalies. For MJO composites, these zonal wind anomalies are averaged by day and then composited over the 46-day time series.

Since the SMART-R rain rate data is hourly, the sounding hour closest to the hour of convective maximum of the Kelvin waves is used for the Kelvin wave sounding composites. Relative humidity is composited for the Kelvin waves to observe the vertical structure of the atmospheric moisture as the events pass over Gan Island. Relative humidity and rain rate lag correlations are also computed for Kelvin waves during each MJO phase using a 3-hour lag. Zonal wind anomalies are also calculated for Kelvin wave composites by centering the data at the hour closest to the convective maximum. Zonal wind anomalies are used to observe the vertical structure of the low-level east-west wind associated with the Kelvin waves (see Figure 2.3, Straub and Kiladis, 2003).

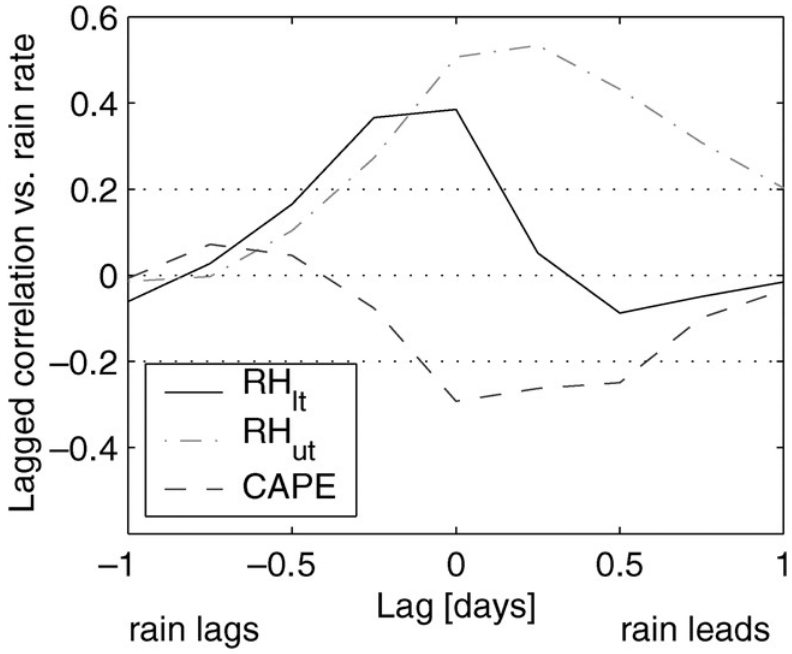

Figure 5.1: Lag-correlation coefficients of lower tropospheric and upper tropospheric relative humidity vs. rain rate at a 6-hourly resolution. From Sobel et al. (2004).

6. RESULTS

6.1 MJO Composite

The MJO event composites are presented as a 46-day time series centered on the day of the OLR minimum of each MJO event (day 0). Composites of the rain rate, rain area, echo-top heights, relative humidity, and zonal wind anomalies are shown to observe the initiation of MJO events and to provide the background atmosphere for passing Kelvin waves. Cloud totals are displayed for the time series to show the evolution of the cloud population during the active MJO.

6.1.1 Rain Rate and Area Composite

Table 6.1 displays the rain totals, percent of stratiform rain, rain area, and maximum percent of radar area coverage for the MJO composite. The precipitation associated with the composited MJO events is presented in Figure 6.1. Lines for convective (solid red) and stratiform (dashed blue) rain are plotted. Figure 6.2 presents the rain area during the composited MJO events.

At day -20, convective (red solid) and stratiform (blue dashed) rain begins to increase with episodes of enhanced rainfall every 2-3 days. This episodic nature of rain is caused by 2-day waves within the MJO (discussed further in Chapter 7). Convective rain reaches its maximum at day -10 and gradually decreases to a minimum at day 7. Stratiform rain reaches its maximum at day -12 and is generally higher than convective rain amounts until day 0. After day 0, stratiform rain contributions become quite low and convective rain dominates. Overall, the stratiform rain fraction is 44.5% during the active MJO (Table 6.1). Stratiform rain area is always greater than convective rain area with maxima of 39.5% and 4.2%, respectively. These values

are lower than the Kelvin wave peaks because of the different temporal averaging (see Section 6.2 and Table 6.1).

Table 6.1: Rain totals during composite MJO event and Kelvin waves.

	Total Rain (mm)	**Stratiform Percent**	**Total Area (km^2)**	**Max Percent of Radar Area**
Kelvin Wave During Active MJO				
Stratiform	18.2	44.6%	146,883	51.4%
Convective	22.6		18,991.4	9.9%
Total Rain	40.7		165,874.4	
Kelvin Wave During Suppressed MJO				
Stratiform	12.3	47.3%	85,936.1	37.1%
Convective	13.7		13,520.7	6.4%
Total Rain	26.0		99,456.8	
Kelvin Wave During Pre-MJO				
Stratiform	19.9	39.4%	142,740	66.0%
Convective	30.5		29,648.5	12.6%
Total Rain	50.4		172,388.5	
Active MJO				
Stratiform	147.9	44.5%	1,204,560	39.5%
Convective	184.3		184,917	4.2%
Total Rain	332.2		1,389,477	

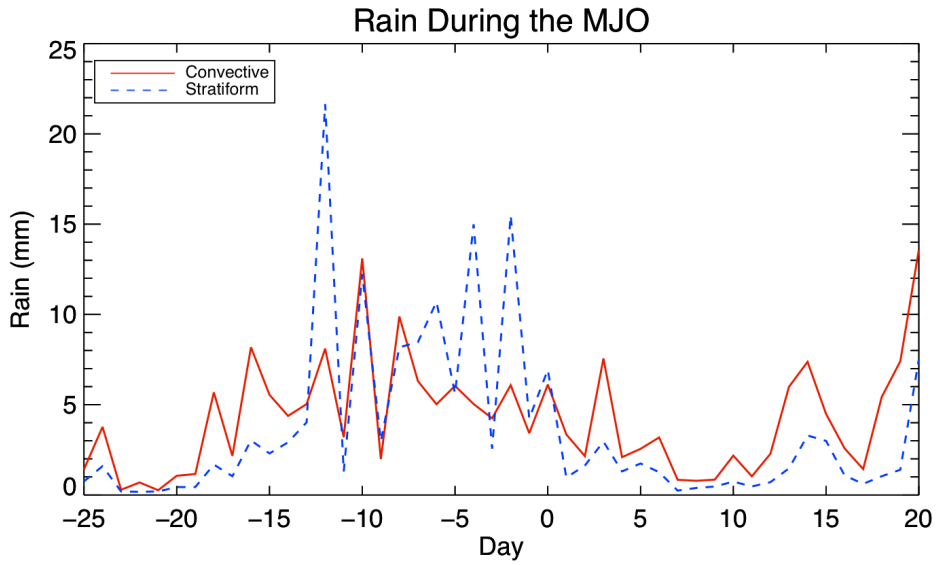

Figure 6.1: Rain accumulation composite of convective (red) and stratiform (blue dashed) rain during the MJO.

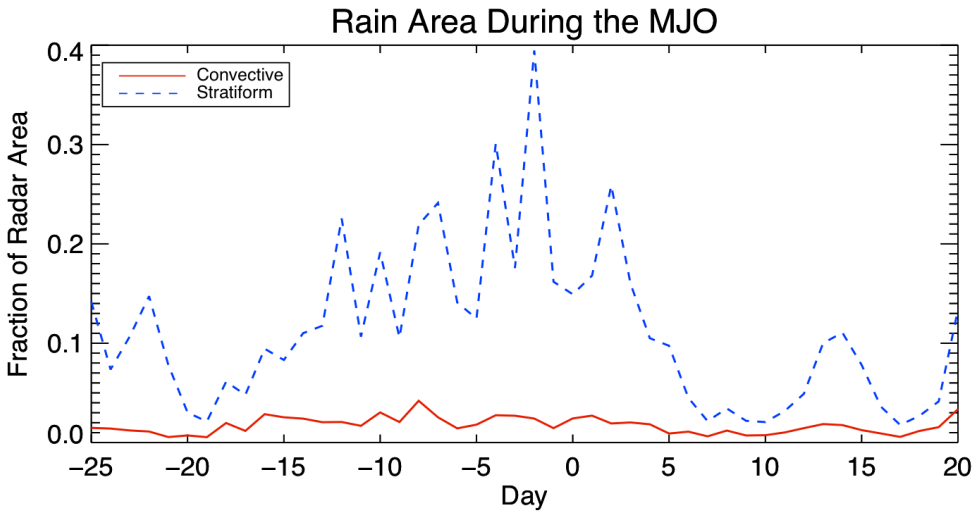

Figure 6.2: Rain area composite of convective (red) and stratiform (blue dashed) rain during the MJO.

6.1.2 Echo-Top Composite

Echo-top composites are presented in Figures 6.3 (convective) and 6.4 (stratiform). The colored contours represent the 10-dBz echo-top counts and indicate

clouds with precipitation-size hydrometeors. The black contours illustrate the 40-dBz echoes, signifying more or larger hydrometeors and more intense rain rates. The tight contours in the convective 40-dBz echo tops represent the most intense convective rain. The tight contours in the 40-dBz stratiform echo tops represent stratiform bright bands. As ice particles fall from freezing temperatures to warmer temperatures, they melt into raindrops. The level at which they melt is detected by the radar as a bright band because the water that forms around the (large) melting ice is highly reflective.

The episodic features seen in the rain rate composite are also evident in the convective and stratiform echo-top counts (Figures 6.3 and 6.4, respectively). Convective and stratiform 10-dBz echoes increase in height beginning at day -20. However, strong convective echoes (as represented by the 40-dBz black contours in Figure 6.3) are present throughout the time series with little noticeable trend. Intense stratiform bright bands occur before and after day 0.

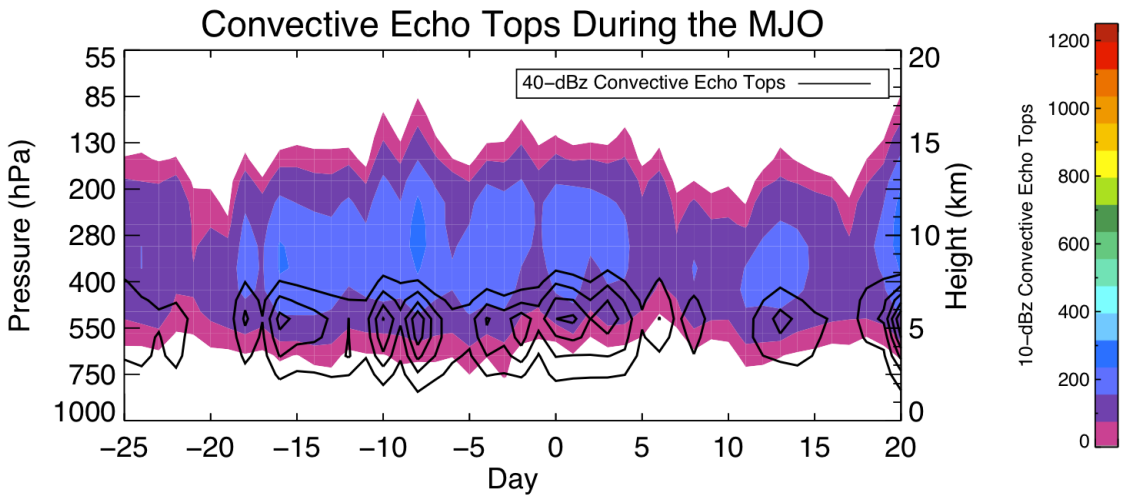

Figure 6.3: Convective echo-top composite during the MJO. Colored contours are the number of 10-dBz convective echoes. Black contours are the number of 40-dBz convective echoes. Echo-tops are averaged by day.

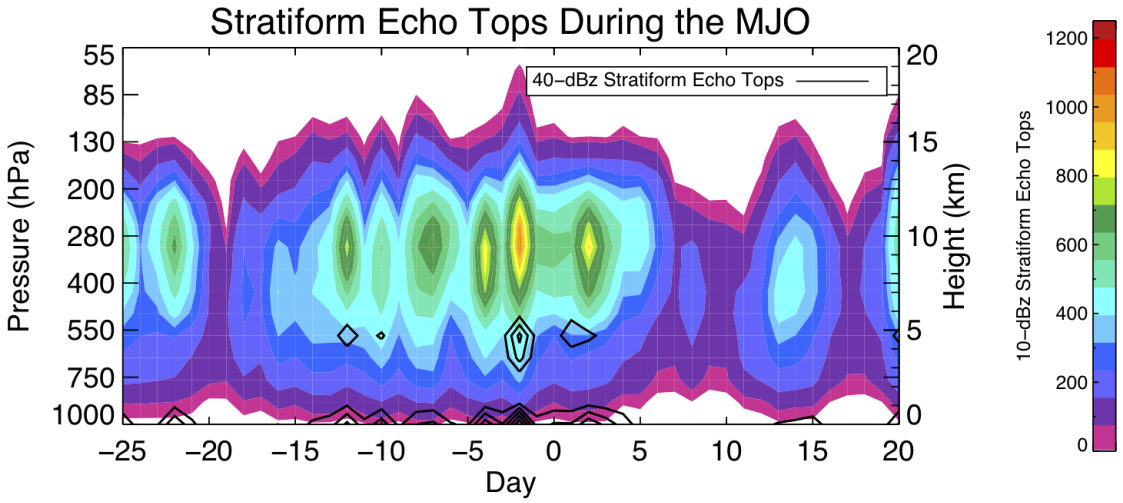

Figure 6.4: Stratiform echo-top composite during MJO. Colored contours are the number of 10-dBz stratiform echoes. Black contours are the number of 40-dBz stratiform echoes. Echo-tops are averaged by day.

6.1.3 Relative Humidity Composite

The relative humidity MJO composite is displayed in Figure 6.5. The warmer colors indicate higher relative humidity, or a moist atmosphere. The cooler colors signify lower relative humidity, or a dry atmosphere. During the active MJO, relative humidity begins to build at low levels around day -20, while the atmosphere at upper levels is very dry. The moisture increases in the upper levels until day 5, after which there is sharp drop in relative humidity throughout most of the troposphere, although low-level moisture persists.

Figure 6.6 displays the lag correlation of total rain accumulation and relative humidity. The black line represents the lower tropospheric relative humidity (700 to 960 hPa) and the red dashed line represents the upper tropospheric relative humidity (200 to 600 hPa). Based on Sobel et al. (2004) (Figure 5.1), lower tropospheric relative humidity is expected to precede the development of convective rain, while upper tropospheric relative humidity is expected to follow the development of stratiform

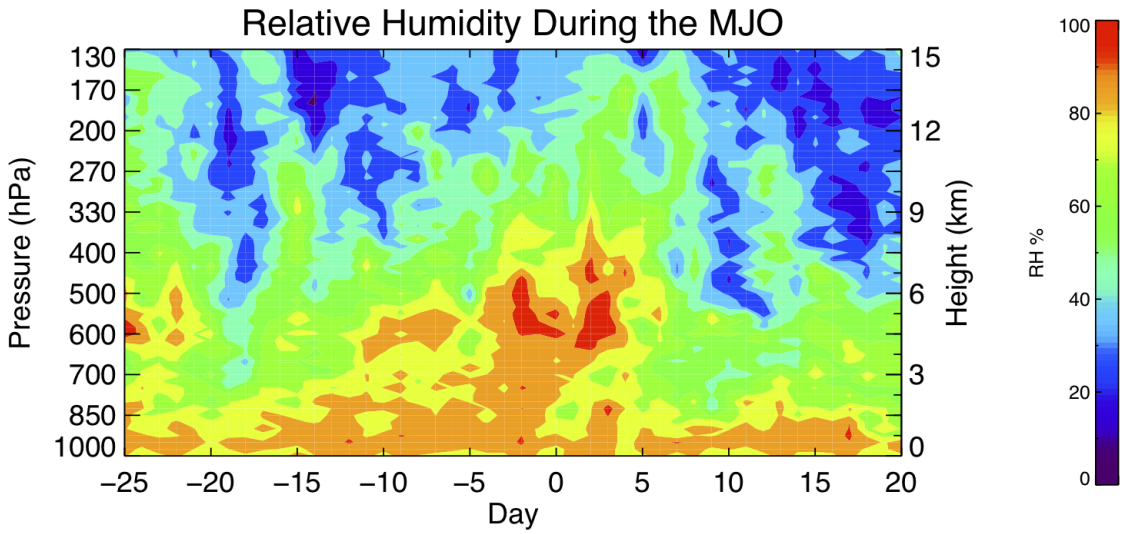

Figure 6.5: Relative humidity composite during the MJO. Warm colors signify high relative humidity (i.e., moist conditions) and cooler colors signify lower relative humidity (i.e., dry conditions).

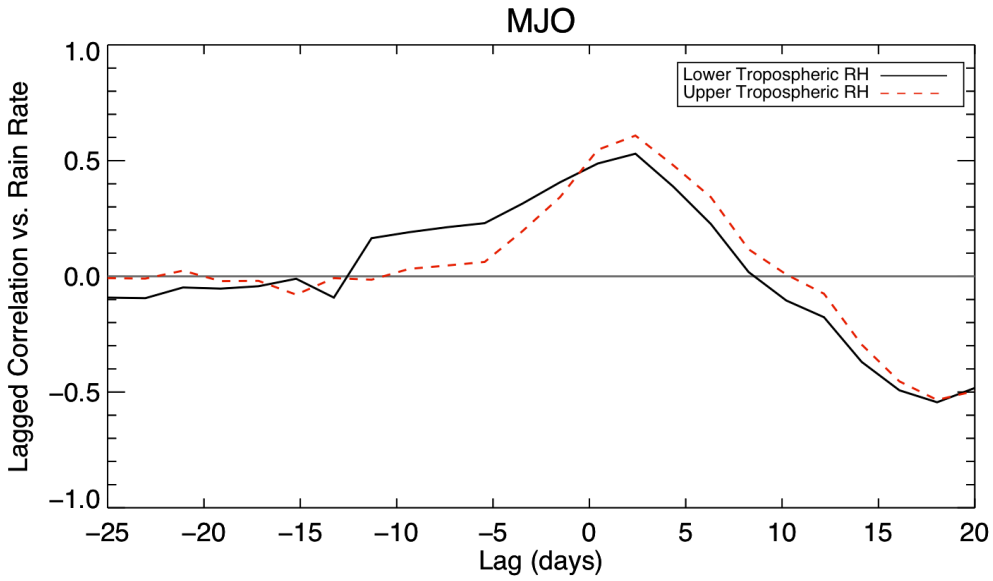

Figure 6.6: Lag-correlation coefficients of tropospheric relative humidity vs. total rain for the MJO. Lower (black) and upper (red dashed) tropospheric relative humidity are plotted at a 1-day resolution.

rain. Lower tropospheric relative humidity is positively correlated with rainfall from day -13 to almost day 10. It peaks right after day 0 and then decreases, consistent

with the development of the active MJO. The upper tropospheric relative humidity correlation with rainfall has a somewhat similar time evolution but is shifted a few days later than the lower tropospheric relative humidity signal.

6.1.4 Zonal Wind Anomaly Composite

Figure 6.7 shows the zonal wind anomalies during the active MJO. Red colors indicate westerly anomalies and blue colors indicate easterly anomalies. Beginning at day -20, easterly wind anomalies form. These easterly anomalies persist until day 0 when there is a sharp shift to westerly wind anomalies throughout much of the troposphere. This signifies the area of convergence. The winds then switch back to easterly anomalies between day 10 and day 15 at all levels. These dramatic tropospheric shifts in wind are not evident in the Kelvin wave passages, perhaps due to the strength of the wind anomalies during the MJO.

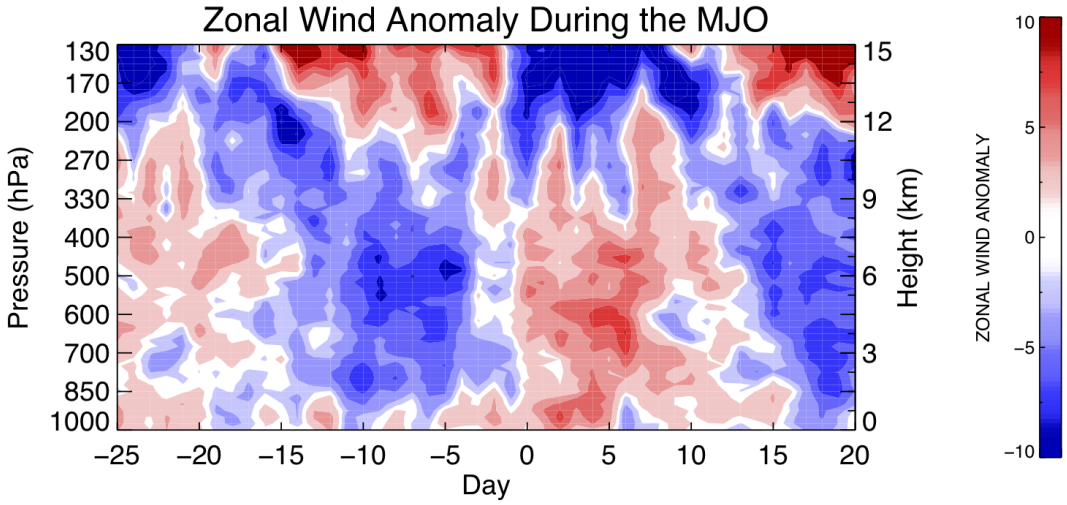

Figure 6.7: Zonal wind anomaly composite during the MJO. Red contours are positive westerly wind anomalies and blue contours are negative easterly wind anomalies.

6.1.5 Evolution of Cloud Population

The KAZR composite MJO cloud population profiles are displayed in Figure 6.8. From day -25 to day -20, clouds above 5 km are numerous but dissipate by day -20 to day -15, consistent with the drying of the atmosphere at low levels (see Figure 6.5). Some upper level clouds are present but significant low-level clouds form after day -15 corresponding to the increase in rain and relative humidity (Figures 6.1 and 6.5). Episodes of shallow convection then mature to the deeper convection evident through day 0. After day 0, deep upper level clouds persist for about 5 days, which corresponds to the high relative humidity present at upper levels (Figure 6.5). Finally, cloudiness decreases at all levels between day 5 and 10, when rainfall, rain area, echo tops, and relative humidity all decrease to a minimum. A small population of clouds between 10-15 days develops at upper levels (most likely stratiform anvil) and lower levels (most likely cumulus congestus) associated with the convective event after the MJO dissolves (evident in rain accumulation and echo tops, Figures 6.1 and 6.3, 6.4 respectively).

6.2 Kelvin Wave Composites

All calculated Kelvin wave composites are presented as a 97-hour time series centered on the hour of maximum convective rainfall for each Kelvin wave. The figures are divided into the active MJO composite, the suppressed MJO composite, and the pre-MJO case depending on when the date of Kelvin wave passage occurs with respect to the MJO events (listed in Table 4.3). Rain rate, rain area, and echo-top composites are presented to show the precipitation characteristics of the Kelvin waves. Relative humidity and zonal wind anomaly composites are also shown to observe the vertical structure of the Kelvin waves. Lag correlations of lower and

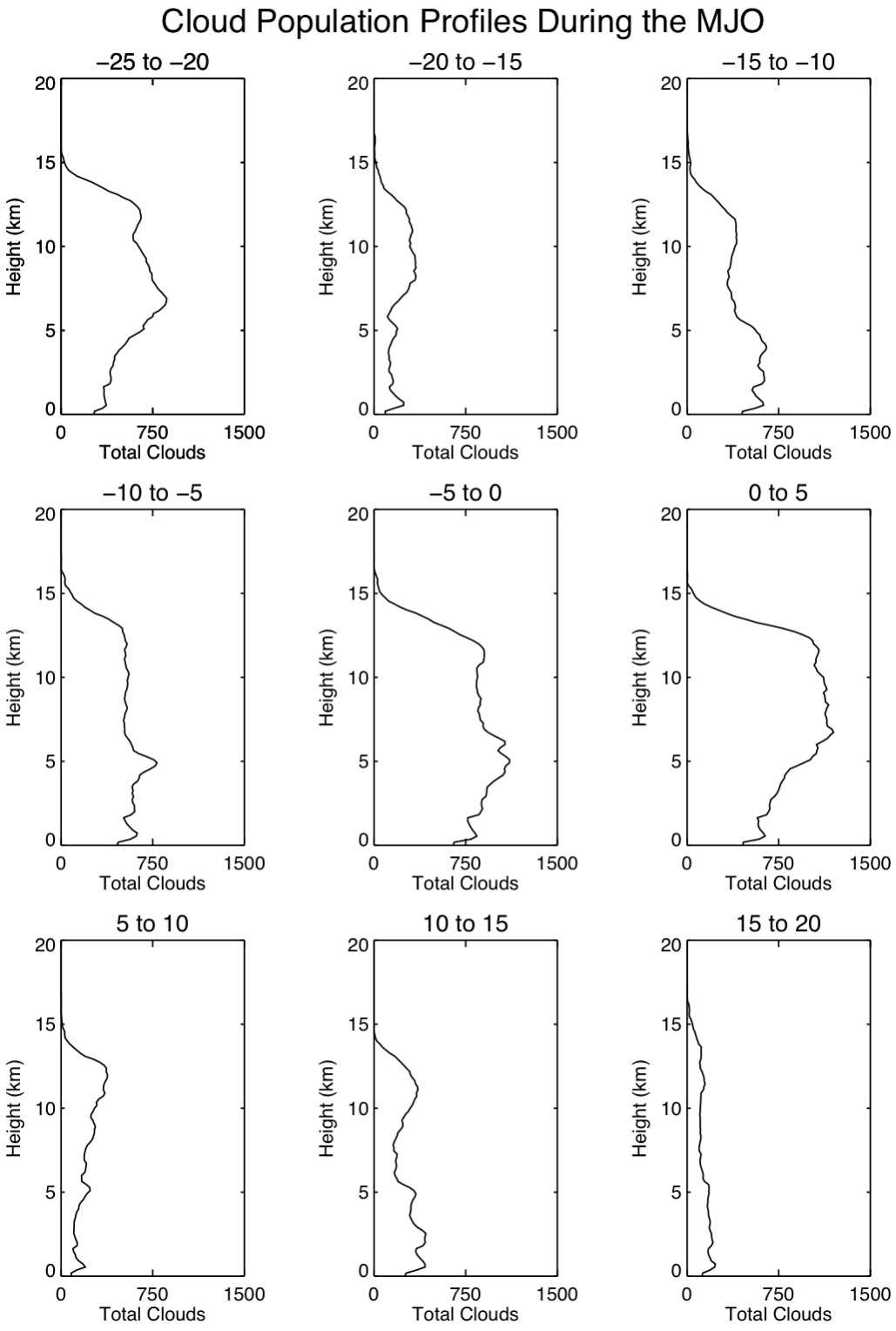

Figure 6.8: Cloud population profiles during the MJO. Computed at 5 days intervals from -25 days to +20 days.

upper tropospheric relative humidity with rain rate are presented to observe the relationship between moisture and rain. Lastly, cloud population profiles are shown to illustrate the evolution of the cloud population.

6.2.1 Rain Rate and Area Composites

Figure 6.9 shows the three rain rate composites and Figure 6.10 shows the three rain area composites for Kelvin waves that occurred during the active, suppressed, and pre-MJO. All of the composites are centered at the hour of convective rain maximum, represented as time zero. Table 6.1 displays the rain totals, percent of stratiform rain, rain area, and maximum percent of radar area coverage for each Kelvin wave composite.

During the active MJO, Kelvin wave rainfall reaches a minimum at -18 hours (Figure 6.9a). At -12 hours, convective rain begins to increase, with a sharp increase within 6 hours of hour 0. Maximum convective rain rates reach 1.3 mm hr^{-1}, the highest of the three composites, after which convective rain rapidly decreases. Convective rain area (Figure 6.10a) is generally small ($< 10\%$ of the radar domain) and shows a similar time progression as convective rain rate. Stratiform rain increases steadily beginning at -12 hours until it reaches a peak 3 hours after the convective maximum (Figure 6.9a). Stratiform rain is greater than convective rain for the next 24 hours. A second stratiform peak develops 12 hours after the convective maximum. This peak is associated with less convective rain than the first peak. Although stratiform rain is present in each individual Kelvin wave used for the composites, the two high peaks in stratiform rain are a result of the November 24 and December 22 Kelvin waves. Overall, the stratiform rain fraction during the Kelvin wave is 44.6% (Table 6.1). As expected, stratiform rain area is higher than convective rain area

during the entire time series (Figure 6.10a) and the two peaks in stratiform rain between hour 0 and hour 24 have the largest area (about 40% of the radar domain).

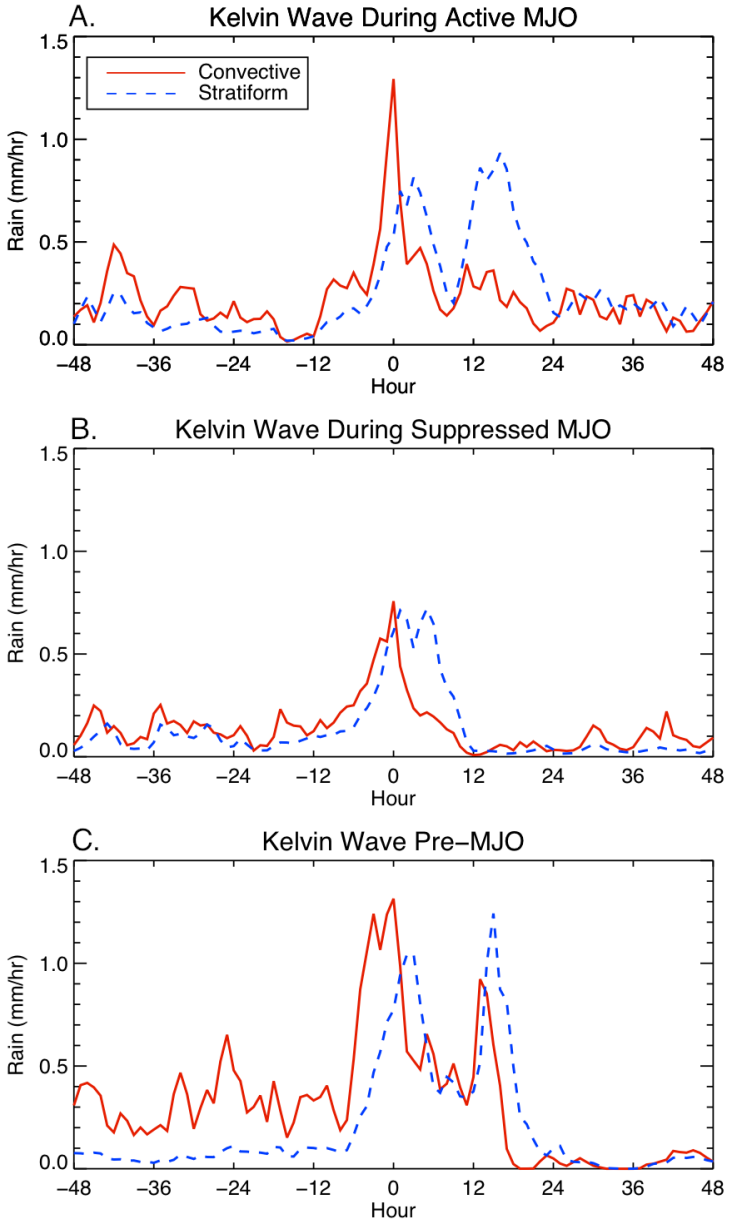

Figure 6.9: Rain rate composites during the Kelvin waves. Red solid lines are convective rain and blue dashed lines are stratiform rain.

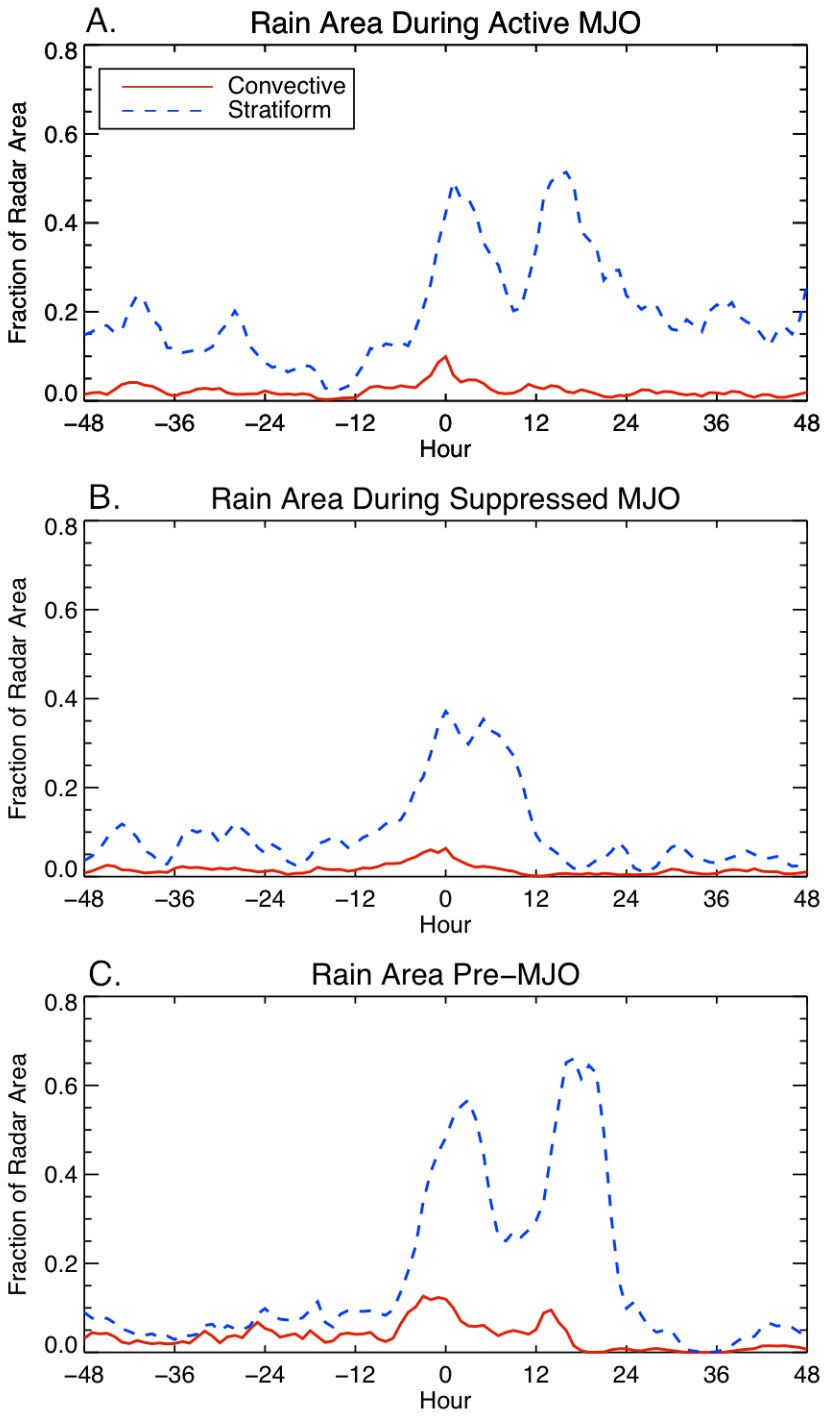

Figure 6.10: Rain area composites during the Kelvin waves. Convective (red) and stratiform (blue dashed) rain areas shown during the active, suppressed, and pre-MJO Kelvin waves.

The magnitude of Kelvin wave rain during the suppressed MJO is noticeably lower than during the active MJO (Figure 6.9b). Beginning at -12 hours, there is a steady build up of convective and stratiform rainfall. After hour 0, the convective rain rate decreases quickly, followed by about 12 hours when there is more stratiform rain than convective rain. The total rainfall decreases and stays at a minimum at +12 hours. Overall, the stratiform rain fraction during the Kelvin wave is 47.3% (Table 6.1). In addition, convective and stratiform rain area evolution mimics the rain rate time series with stratiform rain area higher than convective rain area at all times (Figure 6.10b). Rain totals and area are lower than during the active MJO because of the drier background atmosphere during the suppressed MJO, which makes convective development more difficult (more on this in Section 6.2.3 and Chapter 7).

The rain associated with Kelvin waves during the pre-MJO period (Figure 6.9c) shows a somewhat different time series than Kelvin waves during the active and suppressed MJO. At -8 hours, there is a sharp increase in convective rain, whose peak is maintained for many hours. A second convective rain peak is seen at +14 hours. After hour 0, the stratiform rain becomes greater than the convective rain for three hours. A second stratiform peak develops an hour after the second convective peak. After the second stratiform peak, stratiform rain is greater than convective rain for ten hours. Overall, the stratiform rain fraction during the Kelvin wave is 39.4%, smaller than the active and suppressed MJO Kelvin wave composites (Table 6.1). Stratiform rain area (Figure 6.10c) is higher than convective rain area during the entire time series, though from hour -48 to -24 convective and stratiform rain areas are almost equal. Convective rain area exceeds 10% of the radar domain during peak convective rain times and the two large stratiform area peaks covering about 60% of the radar domain are consistent with the two peaks in stratiform rainfall. The pre-MJO Kelvin wave exhibits the highest amount of stratiform rain and stratiform

area of the three composites. This individual case occurred before the strongest MJO event of the field campaign, which may account for the higher values. Also, since the event is not averaged like the active and suppressed composites, the large variability across the single Pre-MJO event remains.

6.2.2 Echo-Top Composites

Echo-top composites are presented in Figure 6.11 and 6.12 for the convective and stratiform separated echoes, respectively. During the active MJO, Kelvin wave convective 10-dBz echo tops are minimal at -15 hours and increase in occurrence and height through hour 0 (Figure 6.11a). Intense convective echoes (i.e., the 40-dBz echo tops) emerge at -10 hours, but have the highest occurrence and height during the convective rain maximum, suggesting the strongest updrafts and downdrafts are occurring at this time. The convective echo-top counts decrease over the next 6 hours and stratiform echoes begin to dominate (Figure 6.12a), although the strongest bright band signature (as evidenced by the tight 40-dBz contours at mid levels) occurs during the convective rain maximum. The convective echo tops associated with the next rain peak at +12 hours are lower in height and have a weaker 40-dBz signature. A strong bright band signature precedes the majority of the stratiform echo tops (Figure 6.12a), suggesting a different convective system evolution than what occurs at the convective rain maximum at hour 0.

During the suppressed MJO, the Kelvin wave composite shows periodic intense convective outbreaks prior to hour 0 (Figure 6.11b). These outbreaks are sometimes coincident with stratiform rain production or sometimes precede it. Convective 10- and 40-dBz echoes associated with the convective rain maximum begin to develop 12 hours before and maximize in number and height at hour 0 (similar to the active

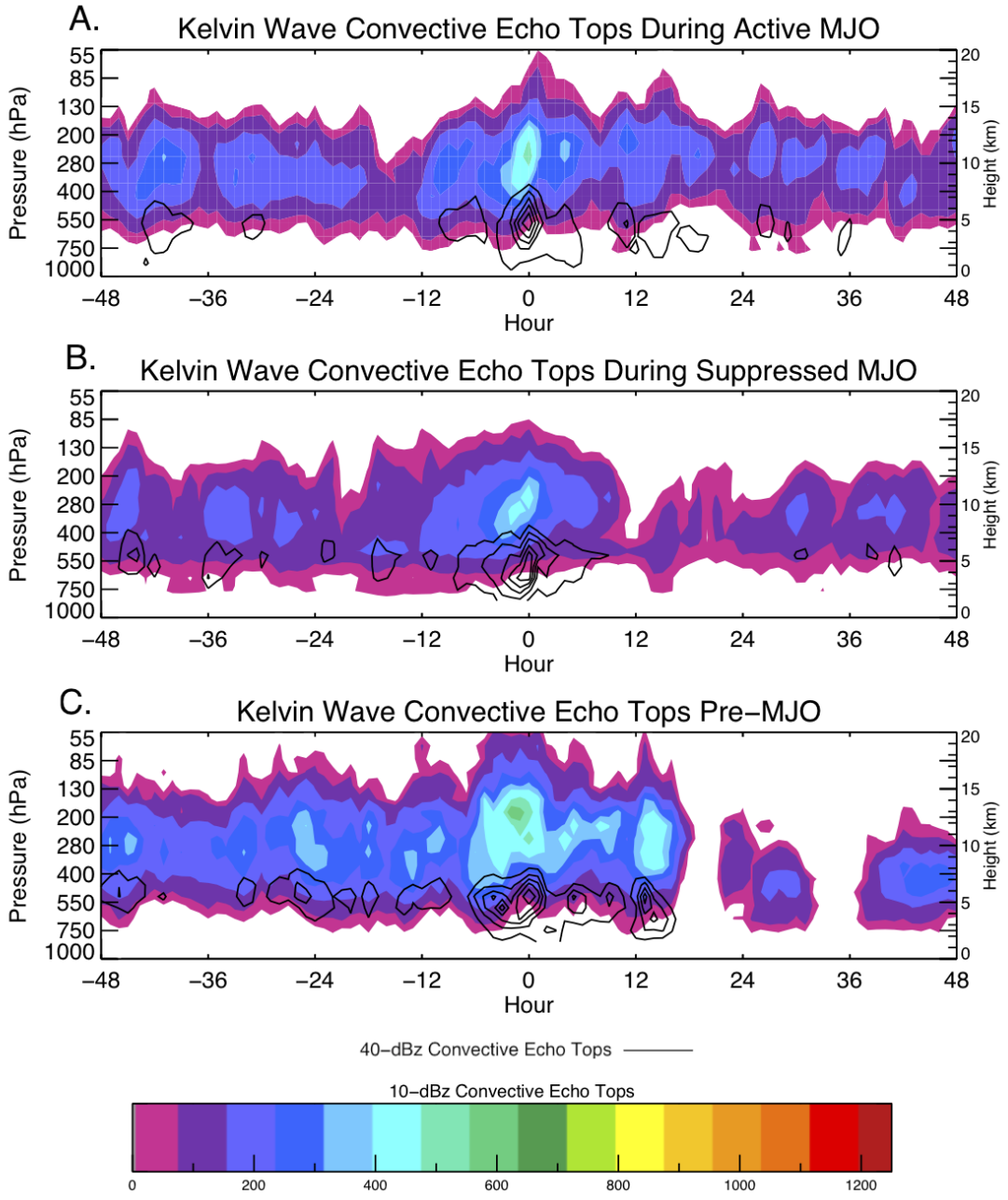

Figure 6.11: Convective echo-top composites during the Kelvin waves. Colored contours are the number of 10-dBz convective echoes. Black contours are the number of 40-dBz convective echoes.

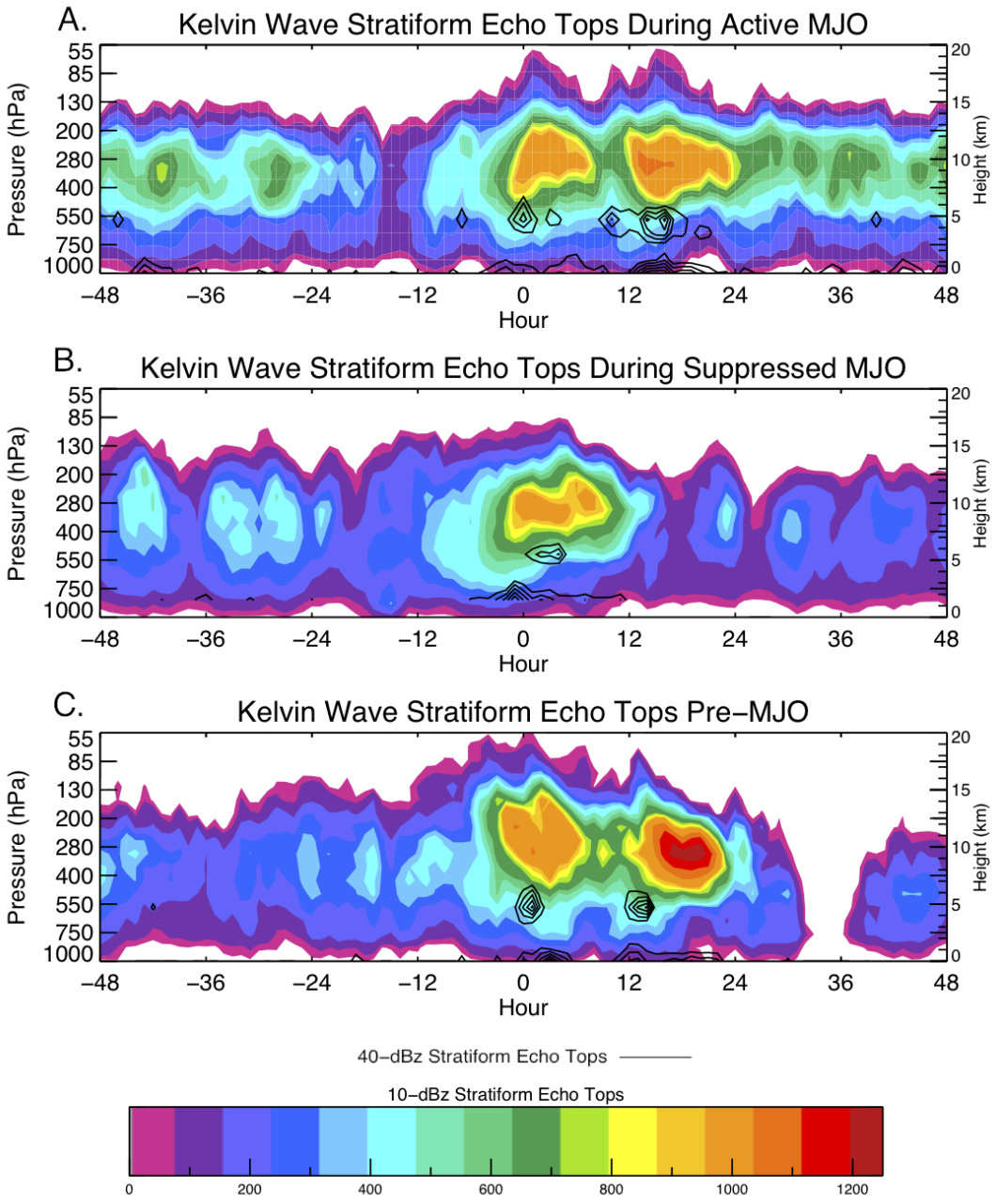

Figure 6.12: Stratiform echo-top composites during the Kelvin waves. Colored contours are the number of 10-dBz stratiform echoes. Black contours are the number of 40-dBz stratiform echoes.

MJO composite). Meanwhile, stratiform echoes develop shortly after the strong convective echoes appear, although the bright band signature lags by a few hours (Figure 6.12b). Both convective and stratiform echoes are present for almost 12 hours after the convective rain maximum until they dissipate, suggesting a continual production of convection to support a robust stratiform region.

The Kelvin wave composites prior to the MJO (Figures 6.11c and 6.12c) also show periodic convective outbreaks before hour 0, but these episodes last longer than during the suppressed MJO and have weaker stratiform echo counts associated with them, perhaps because of the drier upper level environment. The strongest convective echoes do not begin to develop until about 6 hours prior to hour 0, followed by a robust stratiform region. These strong convective echoes weaken and disappear around +12 hours, while the stratiform echoes weaken around +6 hours. At +12 hours, short-lived convective echoes are present with very intense stratiform echoes that persist until +24 hours.

6.2.3 Relative Humidity Composites

Relative humidity composites are shown in Figure 6.13. Relative humidity is expected to be high before the Kelvin wave at low levels and then increase at upper levels as convection develops. After the wave moves through, low-level relative humidity decreases and upper level relative humidity lingers during the stratiform rain and anvil clouds (see Figure 2.3 schematic). Figure 6.14 displays the lag correlation of total rain rate and relative humidity.

The active MJO Kelvin wave composite has high deep tropospheric relative humidity throughout the time series, although relative minima $< 70\%$ exist around 700 hPa before hour 0 (Figure 6.13a). Because of the generally moist atmosphere, there

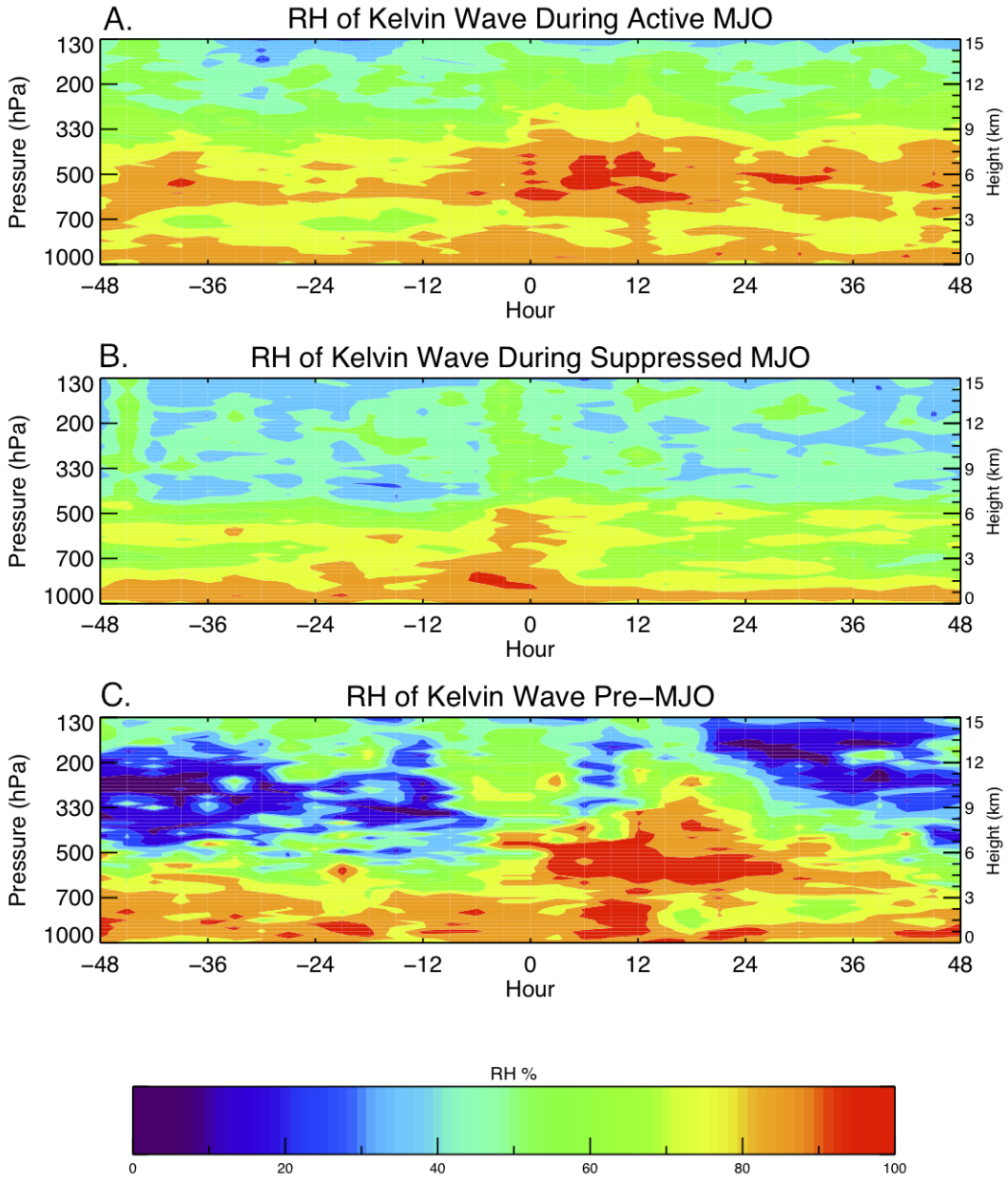

Figure 6.13: Relative humidity composites during Kelvin waves. Warm colors signify high relative humidity (i.e., moist conditions) and cooler colors signify lower relative humidity (i.e., dry conditions).

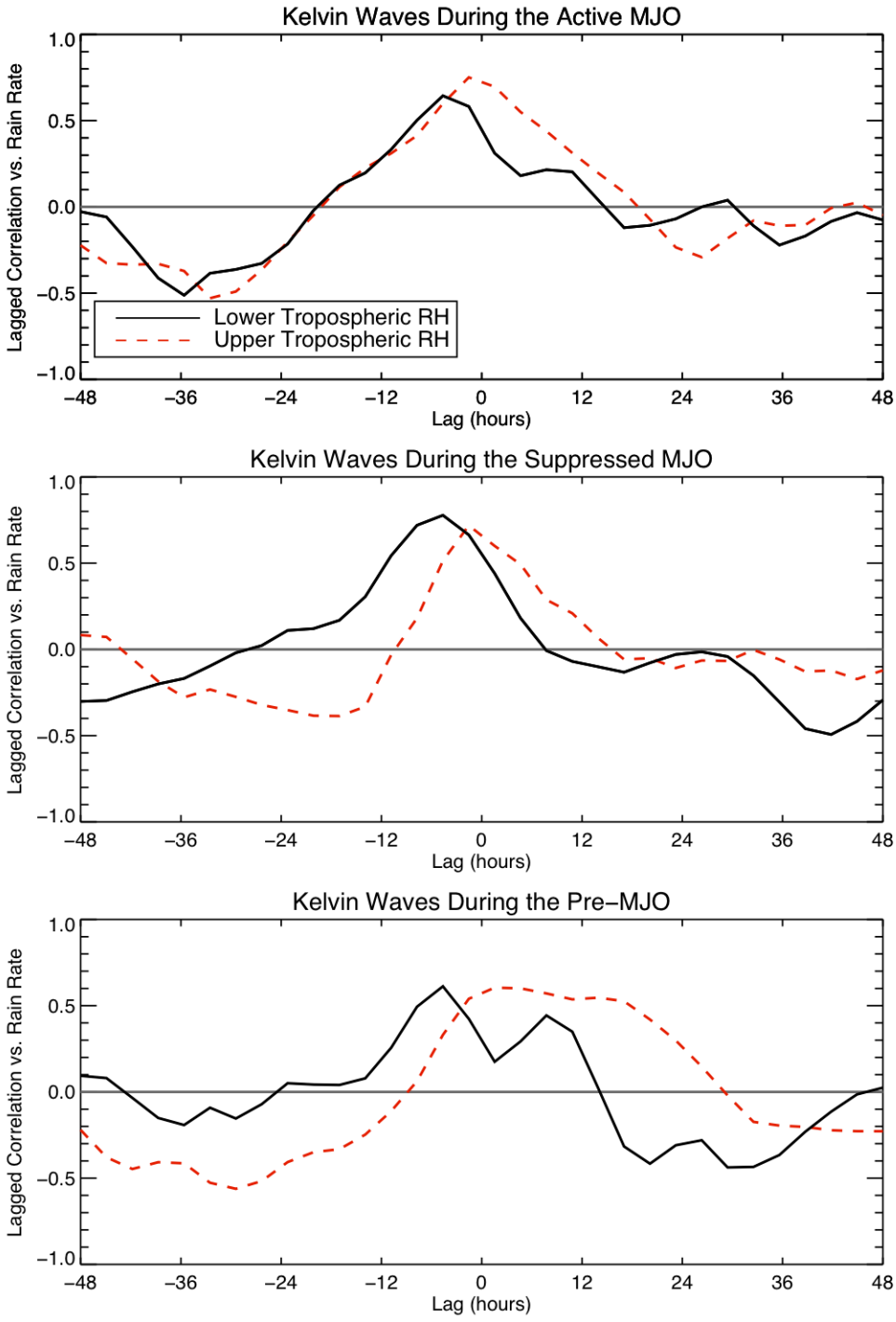

Figure 6.14: Lag-correlation coefficients of tropospheric relative humidity vs. rain rate for the kelvin waves. Lower (black) and upper (red dashed) tropospheric relative humidity is plotted at a 3 hourly resolution.

is no clear build up of moisture prior to the convective rain maximum, however, relative humidity appears to be enhanced at upper levels after hour 0, potentially coincident with the stratiform cloud cover shown in Figure 6.12a. The overall moist profile demonstrates the convective envelope that is associated with the active MJO. Figure 6.14a more clearly shows that the lower and upper tropospheric relative humidity is most negatively correlated (or lowest) 36 to 24 hours before the convective rainfall maximum and becomes positively correlated (or high) starting at hour -20. This signal is consistent with the OLR and sounding-observed specific humidity lag correlations shown in Straub and Kiladis (2002). It is also interesting to note that the ECMWF model did not observe the low-level negative correlations in their case study. The lower tropospheric relative humidity correlation peaks at hour -6, while upper tropospheric relative humidity shows the largest positive correlations with rain rate around hour 0, consistent with Sobel et al. (2004) (Figure 5.1). Lag correlations for lower tropospheric relative humidity decrease to zero by hour 15, while the upper tropospheric relative humidity correlation follows by hour 20.

During the suppressed MJO, there is an apparent moisture increase in the Kelvin wave composite that begins at -12 hours (Figure 6.13b) and is coincident with the convective build up seen in Figures 6.9b-6.11b. The troposphere is relatively dry above 800 hPa until the build up. The atmosphere appears to return to pre-Kelvin wave conditions soon after +12 hours with little signature of upper level moistening associated with stratiform rain and anvil clouds. The relatively dry conditions may be related to the lower rain and rain area coverage produced by the Kelvin wave convective systems during the suppressed MJO. While the large-scale humidity field associated with the passage of Kelvin waves during the suppressed MJO is very different than during the active MJO, the lag correlation of lower and upper tropospheric relative humidity with rain rate (Figure 6.14b) is similar after hour 0. However, there

are no low-level negative correlations before the convective rain maximum and the largest negative correlation for upper level relative humidity occurs much later (i.e., at -12 hours). Thus there appear to be different precursor Kelvin wave interactions with relative humidity during the suppressed MJO.

Prior to the convective rain maximum in the pre-MJO Kelvin wave case (Figure 6.13c), the atmosphere is moist at low levels up to almost 600 hPa but very dry elsewhere. While there is no evident build up much before hour 0, relative humidity is strongly enhanced aloft after hour 0 for about 36 hours, consistent with the extreme stratiform rain displayed in the rain rate and echo-top composites. Drier air occurs at low levels starting at +16 hours. Similar to the suppressed MJO Kelvin wave composite, there is no significant negative low-level relative humidity correlation prior to hour 0 (Figure 6.14c). The lower tropospheric relative humidity correlation starts to increase at hour -12 and remains positive past hour +12, thus lasting longer than the composite Kelvin waves. The lower tropospheric relative humidity correlation also becomes strongly negative after -12 hours, unlike the composites. The upper tropospheric relative humidity correlation is most negative at -36 hours and is positively correlated from hour -6 until well after hour 24. This long period of positively correlated upper tropospheric relative humidity is consistent with the high stratiform rain that exists after hour 0 and differentiates this case from the active and suppressed MJO Kelvin wave composites.

6.2.4 Zonal Wind Anomaly Composites

Figure 6.15 shows the zonal wind anomaly composites for the active, suppressed, and pre-MJO Kelvin waves. A shift from easterly anomalies (blue) to westerly anomalies (red) around 850 hPa is expected and signifies low-level convergence.

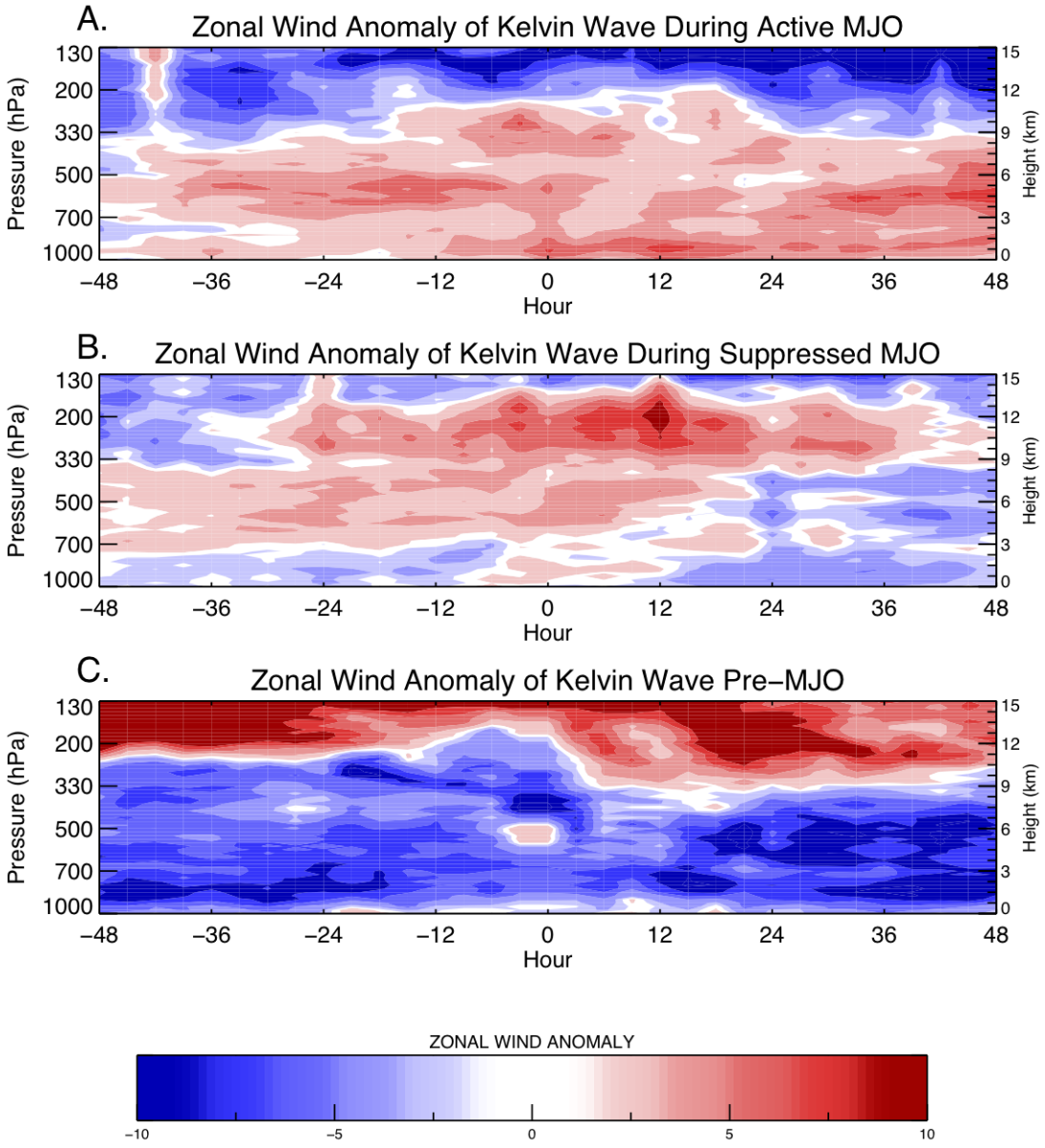

Figure 6.15: Zonal wind anomaly composites during Kelvin waves. Red contours are positive westerly wind anomalies and blue contours are negative easterly wind anomalies.

As shown in Figure 2.1, the low-level winds during an active MJO over the Indian Ocean are strong westerlies converging with easterlies to form deep convection. During the active MJO, the Kelvin wave composite shows low-level easterly anomalies at -48 to -36 hours, but low-level westerly anomalies exist throughout the rest of the composite with some enhancement between -12 and 0 hours (Figure 6.15a). Thus, the 850-hPa wind shift is very weak during the active MJO.

The suppressed MJO Kelvin wave composite displays low-level easterly anomalies for most of the time series (Figure 6.15b). The easterly anomalies extend above 800 hPa at -12 hours with a shift to westerly anomalies soon after, signifying low-level convergence needed for the development of convection. These westerly anomalies are sustained until about +12 hours when the easterly anomalies strengthen again.

Before an MJO event initiates, the background wind is easterly, as displayed in Figure 6.7. During the pre-MJO Kelvin wave strong easterly anomalies dominate most of the troposphere (Figure 6.15c). There is a very subtle surface wind shift that occurs at -24 hours. The surface zonal winds remain weak until +12 hours when easterly anomalies take over again such that a definite area of convergence is unclear.

6.2.5 Evolution of Cloud Population

The composites of cloud population profiles from KAZR are displayed in Figure 6.16. Profiles are shown in 12-hour increments from -36 hours to +36 hours.

During the active MJO, the entire Kelvin wave time series is cloudy (Figure 6.16a), and while low-level cloud cover is sometimes intermittent (in part due to the small spatial scale of shallow convection and the vertically pointing nature of KAZR), a relative minimum in low-level cloud is seen from -24 to -12 hours before the convective rain maximum, while upper level clouds persist throughout the wave

passage. Low level clouds begin to develop from hour -12 to hour 0, followed by an enhancement of cloud cover above 5 km, consistent with SMART-R's stratiform echo-top evolution (Figure 6.11a). Maximum cloudiness throughout the profile persists through +24 hours and then decreases.

Less overall cloud cover is present during the suppressed MJO, as displayed in Figure 6.16b. Lower and upper level clouds exist from hour -36 to hour -24. Very little cloudiness is then evident from hour -24 to hour -12. Clouds develop again from hour -12 to hour 0, at upper and lower levels, excluding development of midlevel clouds (between 5 and 8 km). At hour 0, maximum cloudiness occurs at all levels, consistent with the deep convection and stratiform development seen in rain rate and echo tops (Figures 6.9b, 6.11b, 6.12b). Upper level cloud cover continues through hour 36. Midlevel clouds exist from hour 12 to 24 and are likely non-precipitating altocumulus and altostratus. Cloudiness reaches a minimum after 24 hours where only thin, upper level clouds like cirrus persist.

The single Kelvin wave case during the pre-MJO (Figure 6.16c) shows a different time series than the other two phases. Very little cloudiness exists from hour -36 to hour -12, besides some upper level clouds (most likely thin cirrus). By hour -12 to hour 0, clouds above 5 km begin to develop. Deep convective clouds develop from hour 0 to hour 12 from low levels up to 15 km. This overall cloudiness is maintained until hour 24 when the second peaks in convective and stratiform rain occur (see Figures 6.9c, 6.11c and 6.12c). Clouds dissipate at +24 hours, except for a peak in midlevel clouds around 5 km, suggesting the formation of thin altostratus clouds. Note that the cloud counts seem much greater for this case than for the other two cases. This is because the pre-MJO is not an averaged case, whereas the active and suppressed cases are composited, which causes them to look relatively weaker.

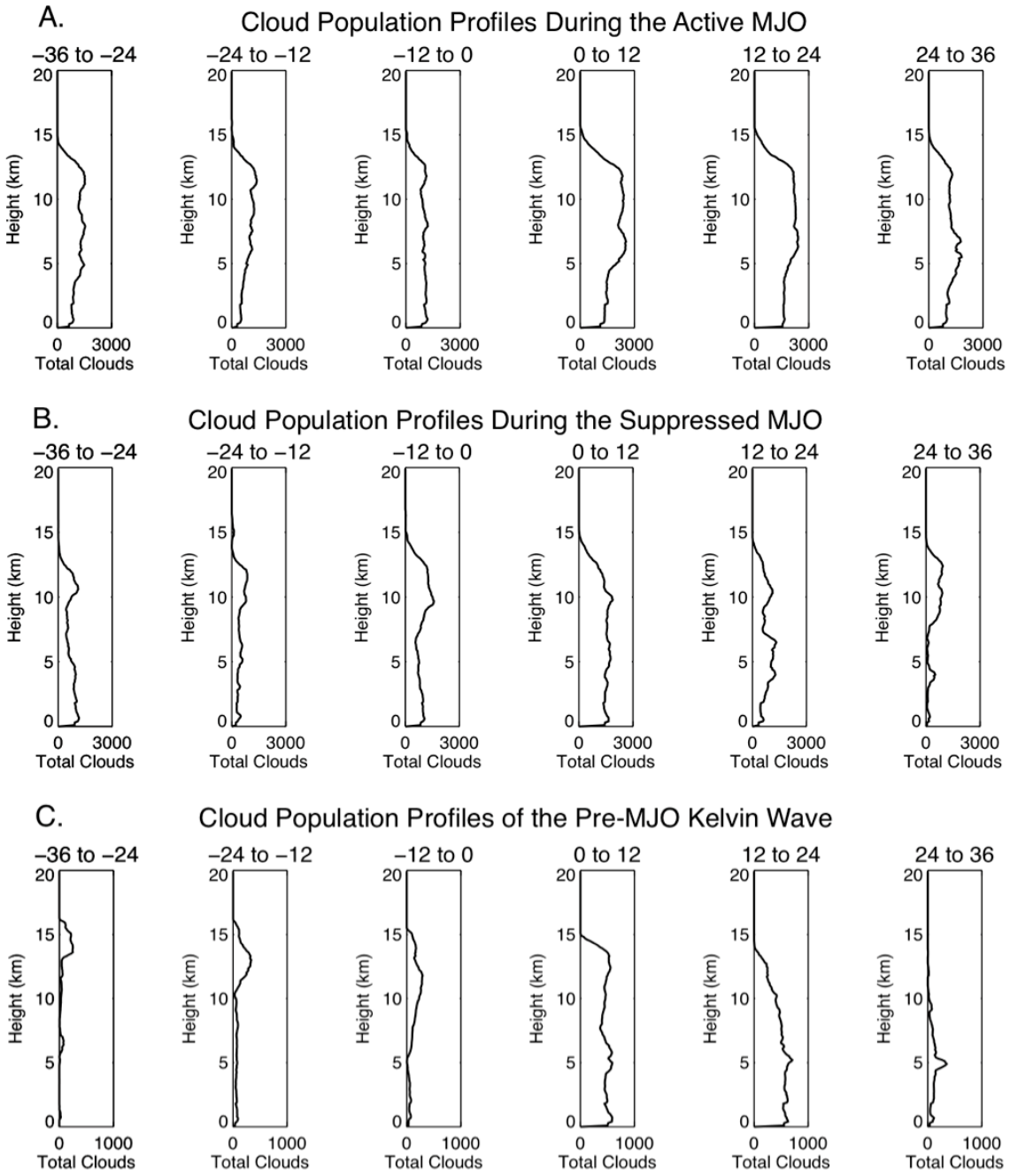

Figure 6.16: KAZR cloud population profiles during the Kelvin waves. Plots are divided into 12 hour sections, from -36 hours to 36 hours.

7. DISCUSSION

7.1 Introduction

During the DYNAMO/AMIE/CINDY2011 field experiment from October 2, 2011 to February 9, 2012, three MJO events and ten Kelvin waves occurred. The high frequency of atmospheric observations during the campaign provided new ways to study MJO initiation in the Indian Ocean. Using radar and sounding data from the experiment, the convection present during Kelvin wave events is analyzed to determine how the waves evolve during the developing, active, and suppressed phases of the MJO. The following section discusses this interaction and the initiation of the MJO based on the results presented in Chapter 6.

7.2 MJO Initiation

The MJO composite illustrates the episodic nature of rain that occurs during the development, maintenance, and dissipation of the MJO as it moves eastward through the Indian Ocean. Two-day convective events have been documented to occur within larger eastward-moving cloud clusters and during the MJO (e.g., Nakazawa, 1988; Madden and Julian, 1994). Figure 7.1a displays the schematic from Nakazawa (1988), which illustrates the movement of the westward cloud clusters within eastward super cloud clusters in the large-scale convective envelope. Another possibility, as Zuluaga and Houze (2013) suggest, is that the episodic nature of the MJO corresponds to the stretching of the convective lifecycle. The 2-3 day convective episodes could also be westward moving 2-day inertia-gravity waves propagating during the MJO (e.g., Haertel and Kiladis, 2004) or even slow, eastward moving Kelvin waves (Masunaga et al., 2006).

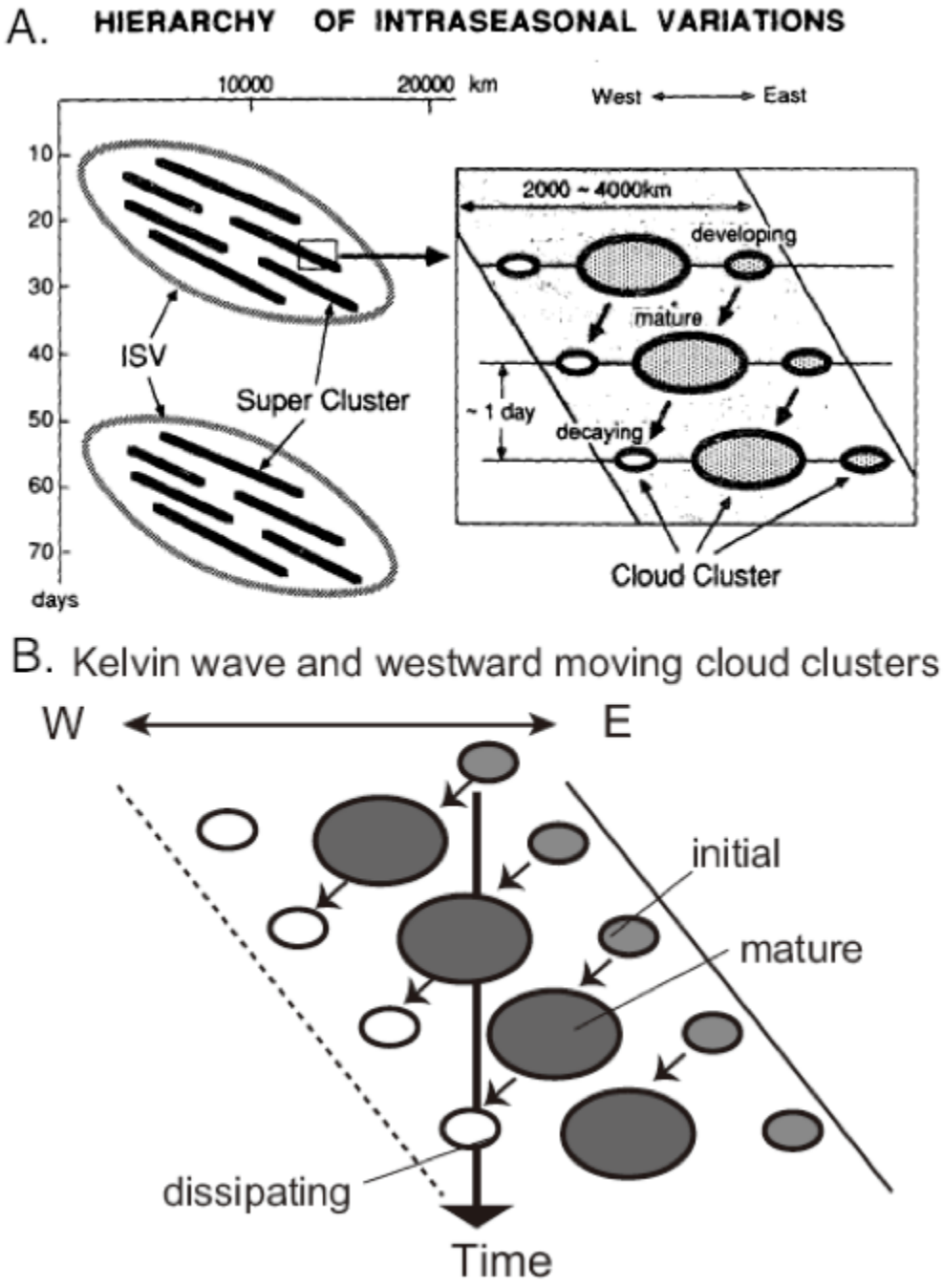

Figure 7.1: The movement of cloud clusters within a) a large-scale convective envelope and b) a Kelvin wave. From a) Nakazawa (1988) and b) Masunaga (2009).

About 15 days prior to the peak MJO date, rainfall, rain area, and echo-top heights begin to increase. As the MJO strengthens, stratiform rain exceeds convective rain. The moisture associated with the MJO builds up from the surface to 350 hPa. The shift in zonal winds is clear at the peak day, signifying convergence. These features are consistent with previous studies and observations of the MJO (e.g., Yanai et al., 2000; Zhang, 2005).

A goal of this thesis is to compare the observations of the MJO onset in the Indian Ocean with current theories of MJO initiation. The discharge-recharge hypothesis for MJO initiation (Blade and Hartmann, 1993; Kemball-Cook and Weare, 2001) suggests that low-level moistening promotes shallow convection, which preconditions the atmosphere for the development of deep convection. The cloud population composite displays the build up of clouds as the MJO strengthens. Beginning at day -15, low- to mid-level clouds are numerous (see Figure 6.8). As the MJO intensifies, deep convection develops and there are more clouds at higher levels. Additionally, the relative humidity composite illustrates the areas of low-level moisture associated with the build up of the MJO. The moisture begins to increase at low levels around 20 to 15 days before the peak day and builds to mid levels between day -15 and -5, until it reaches its peak after day 0. However, the cloud population profiles from the KAZR show little cloud formation until days -15 to -10, suggesting that moisture leads the clouds. Lower tropospheric relative humidity is also positively correlated with rainfall beginning between -15 and -10 days. From these composites, it is likely that the low and mid level moisture initiates the shallow convection which then develops into deep convection present from day -5 to +5.

The convectively coupled Kelvin waves that occurred during suppressed MJO events have the typical structure documented by previous studies. The active MJO provides a moisture-rich convective envelope, which supports the development of

deep convection. The convection of Kelvin waves that occurred during the active MJO is thus enhanced because of this environment. Additionally, because of the size and strength of the MJO, the active MJO suppresses the vertical structure of the passing Kelvin wave. This makes it difficult to identify Kelvin waves during the active MJO using features like an 850 hPa wind shift or vertical moisture increases. A more in depth discussion of these events is presented in Section 7.3.

For MJO initiation, the most important Kelvin wave is the one that occurs during the developing phase of the MJO. The single case examined in this thesis shows an intense convective event followed by substantial stratiform rain and a second convective/stratiform event starting 12 hours later. Before the wave, the upper atmosphere is very dry, and as the wave passed, upper level relative humidity increases and is maintained after the event. This continued moisture could help provide the large-scale moisture field necessary to organize convection beyond the mesoscale during the active MJO. As suggested by the frictional Kelvin-Rossby wave-CISK theory of MJO initiation, a globally circling Kelvin wave could initiate the MJO by providing low-level moisture convergence. This pre-MJO Kelvin wave does provide some increased low-level relative humidity after +36 hours, but the winds remain as strong easterly anomalies.

7.3 Kelvin Waves and the MJO

Kelvin waves that occurred during the suppressed, active, and developing phases of the MJO display different convective and stratiform rainfall, rain area, and echo-top height evolution, as well as distinct variations in vertical profiles of relative humidity and zonal wind anomalies. A comparison with the convectively coupled Kelvin wave schematic by Straub and Kiladis (2003; hereafter, SK03) is made with

each phase to demonstrate the differences and similarities of the structures. Results from the following studies are discussed with respect to the results presented in this thesis: MISMO observations of eastward propagating convective systems (EPCSs) that resemble Kelvin waves (Katsumata et al., 2009; Yamada et al., 2010), eastern Pacific Kelvin wave studies by Straub and Kiladis (2002; 2003), and climatologies of Kelvin waves during active and suppressed MJO (Roundy, 2008; MacRitchie and Roundy, 2012).

7.3.1 Suppressed MJO

When the MJO is suppressed, the structure of Kelvin waves in the Indian Ocean is consistent with the SK03 schematic, shown in Figure 2.3. The shift from easterly wind anomalies to westerly anomalies at low levels exists, forming an area of low-level convergence. The same low-level wind shift is evident in the EPCSs during MISMO (Katsumata et al., 2009; Yamada et al., 2010). This convergence occurs about 12 hours prior to the maximum convective rainfall and helps develop the convection associated with the Kelvin wave passage. Before the Kelvin wave passes, high relative humidity extends to upper levels. After the wave passes, relative humidity decreases. A similar composite is evident from the Yamada et al. (2010) study of four EPCSs during the MISMO campaign, showing an increase in relative humidity as the systems pass.

The Kelvin waves during the suppressed MJO are associated with an increase in both convective and stratiform rain, which lasts for about 24 hours and is centered on hour 0. For the 12 hours before hour 0, stratiform rain lags convective rain by about an hour. After hour 0, stratiform rain dominates the total rainfall until both the stratiform and convective rain dissipates. The large amount of stratiform rain and

rain area trailing the convective event is consistent with the evolution of organized tropical convective systems, also called mesoscale convective systems (Houze, 2004). In addition, there is less stratiform rain and less pronounced stratiform echoes than during the active MJO, which is inconsistent with the suggestion that during the suppressed MJO, the stratiform rain clouds are stronger and more abundant than during the active MJO, from the Roundy (2008) climatology study. This inconsistency could be due to the Kelvin waves moving slower through the active MJO than during suppressed conditions, allowing more stratiform rain to develop out of the high amounts of deep convection. There is also less rain during the suppressed MJO Kelvin waves than during the active MJO Kelvin waves (see Table 6.1), however, the stratiform rain percent is higher during the suppressed MJO (47.3%) than during the active MJO (44.6%), demonstrating that stratiform rain accounts for more of the total rain during the suppressed MJO. Kelvin waves during the suppressed MJO could have more stratiform rain than during the active MJO because the suppressed Kelvin waves initiate in a drier background environment than the active Kelvin waves. This inhibits the development of large amounts of convective rain, which can otherwise form more easily during the moist envelope of the active MJO. Kelvin waves are less frequent and weaker during austral summer (Masunaga, 2007), which could also account for the small amount of rainfall associated with these Kelvin waves.

There seems to be a distinct relationship between relative humidity and development of convective and stratiform rain. Lower tropospheric relative humidity is positively correlated with the build up of convective rain. The most positive correlation between lower tropospheric relative humidity and rain rate occurs about three hours before the convective maximum, suggesting that low-level moistening precedes deep convection by about three hours. Upper tropospheric relative humidity is most positively correlated with rain rate at hour 0, showing that upper tropospheric rel-

ative humidity precedes peak stratiform rain by at least one hour (based on the stratiform rain peak in Figure 6.9b), which is different than the Sobel et al. (2004) study and the other Kelvin wave composites. This difference could suggest that the precipitation structure of the Kelvin waves during the suppressed MJO are not like typical mesoscale convective systems, in that high upper level relative humidity supports the development of stratiform rain, instead of the reverse. However, the temporal differences when matching the hourly rain rate products to the closest 3-hourly sounding observations could also account for this difference. Hourly soundings in the future field campaigns or utilizing model and reanalysis profiles should remedy this bias to determine if the lag found here is valid.

7.3.2 Active MJO

During the active MJO, the documented structure of the Kelvin wave (SK03 schematic) is no longer apparent. The winds exhibit consistently strong westerly anomalies at low levels. Since the active MJO creates a moist convective envelope that propagates eastward, the relative humidity is high throughout the free troposphere. However, the lag correlation displays a result similar to Sobel et al. (2004) for large-scale deep convection, where upper tropospheric relative humidity correlations lag the lower tropospheric relative humidity correlations with rain rate. There is less of a positive correlation in the build up of convective rain than the suppressed MJO case. In other words, since the troposphere is very moist throughout the active MJO, the gradual increase in positively correlated lower tropospheric relative humidity and rain rate observed during the suppressed MJO Kelvin wave does not occur during the active MJO. The most positive correlation in lower tropospheric relative humidity with rain rate for Kelvin waves during the active MJO is before

hour 0. This shows that since the relative humidity is high during the active MJO, the higher values of relative humidity precede the sudden maximum in convective rain. Upper tropospheric relative humidity is most positively correlated around hour 0, demonstrating that the stratiform rain peaks are likely responsible for keeping the upper levels of the troposphere moist. The wind anomalies and moisture signatures typically associated with a convectively coupled Kelvin wave are absent. The large, strong active MJO events seem to suppress the vertical structure that is expected with Kelvin waves.

The convective rainfall during the active MJO Kelvin wave composite is much larger than during the suppressed MJO Kelvin wave composite, and is followed by two peaks in stratiform rain. This greater convective rainfall could develop because the MJO provides an already moist atmosphere, which is favorable for convection formation and maintenance. The rain from the active MJO Kelvin wave passage lasts for about 36 hours, which is 12 hours longer than the suppressed MJO composite. This suggests that Kelvin waves move slower through an active MJO than in suppressed conditions, consistent with the findings of the Roundy (2008) climatology study. The dual peaks in stratiform rain during the active MJO Kelvin wave could be multiple 1-2 day westward-moving cloud clusters that make up the Kelvin wave convection (Nakazawa, 1988; Straub and Kiladis, 2002; Masunaga, 2009). An example of how these cloud clusters move through the Kelvin wave is shown in the schematic in Figure 7.1b, from Masunaga (2009). Since Kelvin waves generally move slower through the active MJO than in suppressed conditions, more than one cloud cluster can develop and be observed over Addu Atoll.

However, the amount of convective and stratiform rain during an active MJO that occurred also during a Kelvin wave is much less than documented in MacRitchie's and Roundy's (2012) climatology study using TRMM rainfall estimates. Table 7.1

Table 7.1: Composite Kelvin wave rain statistics during the active MJO.

	MJO	Kelvin wave	Kelvin wave Percent of MJO
Average Accumulated Rain			
Convective Rain (mm)	47.73	9.75	20.42%
Stratiform Rain (mm)	54.17	9.48	17.49%
Total Rain (mm)	101.89	19.22	18.87%
Average Rain Area			
Convective Area (km^2)	42,026.16	8,010.15	19.06%
Stratiform Area (km^2)	410,607.64	84,720.48	20.63%
Total Area (km^2)	452,633.80	92,730.64	20.49%
Average Rain Rate			
			Percent Higher than MJO Rate
Convective Rain Rate (mm hr^{-1})	0.21	0.41	96.14%
Stratiform Rain Rate (mm hr^{-1})	0.26	0.39	54.51%
Total Rain Rate (mm hr^{-1})	0.46	0.80	73.07%

shows the convective and stratiform rain totals on days when the filtered OLR is below the -10 Wm^{-2} threshold for the three MJO events and the four Kelvin waves. Using TRMM satellite observations, MacRitchie and Roundy (2012) showed that 62% of total rainfall during an active MJO is attributed to passing Kelvin waves in the Indian Ocean. Rain from the passing Kelvin waves only accounts for about 19% of the total rainfall during the three DYNAMO MJO events, about two thirds less than what MacRitchie and Roundy (2012) reported. This difference could be attributed to the spatial differences between Roundy's global study and this local

study. Additionally, Kelvin wave rain area accounts for about 20% of total MJO rain area whereas MacRitchie and Roundy (2012) found that Kelvin waves were responsible for 46% of the total MJO rain area. They also reported that rain rates were 60% higher when a Kelvin wave passed through an active MJO event. Similarly, this study shows that rain rates are actually about 73% higher when Kelvin waves occurred during the active MJO. The lower total rainfall and rain area contributed by Kelvin waves could be attributed to the small number of events sampled for this thesis as opposed to the ten years of data used in their climatology study, differences between ground-based radar observations and TRMM satellite rain estimates, or the different latitude and longitude domains of the two studies (5°N to 5°S, 65°E to 115°E in Roundy, 2008 vs. 10°N to 10°S, 72.5°E to 75°E in this thesis).

The cloud population profiles show a more pronounced evolution than during the suppressed MJO. The overall time series is much cloudier. In addition, cloudiness peaks at upper levels (between 5 and 13 km) during the active MJO Kelvin wave composite due to the high relative humidity throughout the profile, which keeps the atmosphere moist and supports the development of deep convection, stratiform rain, and anvil cloud. The stratiform clouds are more amplified during the active MJO than during the suppressed MJO, which disagrees with the suggestion of the opposite case by Roundy (2008).

7.3.3 Pre-MJO

The pre-MJO case displays a combination of the active and suppressed MJO-Kelvin wave composites. A sharp increase in convective rain begins at hour -6 and is followed by two high peaks in stratiform rain, which are greater than the stratiform rain associated with the two composites. The entire event lasts for about 30 hours,

which is shorter than during the active MJO and longer than during the suppressed MJO. This suggests that the speed of the pre-MJO Kelvin wave is slower than during the active MJO but faster than during the suppressed MJO. Again, the two convective/stratiform peaks could be due to embedded cloud clusters within the slower-moving Kelvin wave event, similar to the active MJO case (Figure 7.1b). The cloudiness observed by the cloud radar shows no low-level cumulus build up to the convective rain maximum, which may be in part due to the decreased sampling by the vertically pointing KAZR. The large area of upper level stratiform cloud and deep convective clouds after hour 0, however, is similar to the observations of stratiform rain at SMART-R.

The pre-MJO Kelvin wave event displays the expected relative humidity structure, where moist air exists at low levels before the wave passage and increases at upper levels after the passage, as shown by the SK03 schematic and by the pre-MJO event from MISMO (Katsumata et al., 2009; their EP3), though this increase is rapid. The lower tropospheric relative humidity is most positively correlated with rain rate three hours prior to the convective maximum, suggesting that relative humidity precedes the onset of intense convective rain by three hours, similar to the suppressed MJO case. A second smaller peak in positive correlated lower tropospheric relative humidity occurs nine hours after the convective maximum, which suggests that rain could lead the increase in relative humidity. After the wave passage, relative humidity remains high except for a dry layer around 800 hPa. This lingering moisture could precondition the atmosphere for the onset of the MJO. The upper tropospheric relative humidity is positively correlated with rain rate for the longest time of the three cases, which closely follows the upper tropospheric relative humidity correlations from Sobel et al. (2004). As expected, this lag is a result of stratiform rain (relative humidity lag with stratiform rain not shown).

Zonal wind anomalies show very little evidence of a low-level wind shift. The average zonal winds from three sounding locations during MISMO also show no low-level wind shift for the EPCS that occurred pre-MJO (Katsumata et al., 2009). However, observations of the bandpass filtered soundings from only Gan Island showed a clear shift in the winds at low levels.

The Masunaga (2007) climatology study on MJO and Kelvin waves found that the MJO is typically preceded by a Kelvin wave in boreal winter (December, January, February). The particular pre-MJO event during DYNAMO occurred in November, during boreal fall. Additionally, a pre-MJO Kelvin wave was absent before the December MJO, which disagrees with Masunaga's (2007) climatology. This difference is attributed to the small number of events sampled.

The cloud population profiles illustrate little to no clouds at all levels from hour -36 to hour 0, except for some thin, upper level clouds. There is no shallow convection developing into deep convection. Additionally, 24 hours after the convective maximum, cloudiness becomes sparse. Although a peak in thin midlevel clouds forms at the end of the time series, shallow convection provided by the Kelvin wave to initiate the MJO is absent. Since the lifecycle of convective systems typically ends with stratiform rain leading to extinction, it is unlikely that shallow convection would develop due to a Kelvin wave passage.

8. CONCLUSION

The purpose of this thesis was to examine the MJO onset and the convection present during Kelvin wave events to determine how they interact with the developing, active, and suppressed phases of the MJO using recent observations from a field campaign in the Indian Ocean. MJO events and Kelvin waves were identified using three wavenumber-frequency filters of satellite-retrieved OLR. The filtered data were averaged from 10°N to 10°S latitude and 72.5°E to 75°E longitude to identify the events that passed over Addu Atoll, Maldives. An OLR threshold of -10 Wm^{-2} was applied to choose the strongest events.

Radar and sounding observations from the DYNAMO/AMIE/CINDY2011 field campaign were used to observe the precipitation characteristics, cloud populations, and atmospheric profiles associated with the identified events. Composites of four and five Kelvin waves that occurred during the active and suppressed phases of the MJO, respectively, were calculated by centering the wave passage on the hour of maximum radar-observed convective rain. An individual case of a Kelvin wave that occurred during the pre-MJO phase was also examined. The three MJO events that occurred in October, November, and December were composited by centering the events on the minimum OLR day.

Radar products used in this thesis were convective and stratiform separated rain rate, rain area, and echo-top heights from the SMART-R precipitation radar on Addu Atoll. The evolution of cloud populations was examined by using the cloud boundary measurements from the KAZR cloud radar. Atmospheric profiles of relative humidity and zonal wind anomalies from three-hourly soundings on Gan Island were used to study the vertical profiles during the events.

Kelvin waves that occurred during the suppressed MJO displayed a vertical structure consistent with observations from previous studies. There was a clear low-level wind shift signifying convergence, along with vertical relative humidity increases and subsequent atmospheric drying. Maximum convective rain rate lagged lower tropospheric relative humidity by three hours, while upper tropospheric relative humidity followed the development of stratiform rain. The convective rain lasted for about 24 hours, with the peak at 12 hours. Stratiform rain was present following the convective rain. These Kelvin waves formed in a drier atmosphere than during the active MJO. Hence, these waves were convectively weaker.

The moisture-rich atmosphere provided by the active MJO enhanced passing Kelvin waves. These waves had large amounts of convective rain, and the event lasted about 36 hours, suggesting a slower moving wave than during suppressed MJO conditions. Two peaks in stratiform rain followed the convective rain, which could be evidence of westward moving cloud clusters within the Kelvin wave. More upper level clouds were present during the active MJO Kelvin waves than during the suppressed MJO due to the extent of high relative humidity. The strength of the MJO masked the changes in atmospheric profiles expected for the Kelvin wave passages.

The pre-MJO Kelvin wave formed in a very dry environment. Relative humidity built from low levels during this event, although a low-level wind shift was absent. Convective rain reached its peak quickly, and peaked again after 12 hours. A peak in stratiform rain followed each convective peak, similar to the active MJO Kelvin waves, again suggesting embedded cloud clusters. Upper tropospheric relative humidity was positively correlated when it preceded rain rate for the longest of the three cases, demonstrating that the upper troposphere remained moist, as a result of the stratiform rain. The moisture from this event was also maintained at low levels after

the wave passed and provided necessary large-scale humidity to promote convection and may have influenced the onset of the MJO. To validate this initiation, a closer look at the MJO onset is needed. For example, identifying the relative humidity associated with the pre-MJO Kelvin wave and the relative humidity coincident with MJO initiation, if possible, would support or discount this idea. However, challenges due to the temporal scale of the soundings make this task difficult. Additionally, observing atmospheric profiles from different locations within the study domain may give more insight into the distributions of moisture leading an MJO event.

Two of the many theories of MJO initiation were discussed in this thesis. The discharge-recharge theory suggests that that low-level moistening promotes shallow convection, which preconditions the atmosphere for the development of deep convection. The frictional Kelvin-Rossby wave-CISK theory suggests that Kelvin waves provide boundary-layer moisture convergence to the east of MJO convection. The moisture remaining after the passage of the pre-MJO Kelvin wave could support these theories, although evidence of shallow convection forming 24 hours after this event was absent, as expected for the discharge-recharge theory. However, the cloud population during the active MJO displayed low- and mid-level clouds leading to deeper convection and the peak of the MJO. Relative humidity also built from these low to mid levels as the MJO intensified. The low-level moisture and shallow convection leading the active MJO support the development of the deep convection associated with the MJO, consistent with the discharge-recharge theory of initiation.

The mechanisms behind the onset of the MJO are becoming clearer due to radar and sounding observations during DYNAMO/AMIE/CINDY2011, however, a longer time series of data would provide stronger explanations for this phenomenon. Satellite observations have provided an innovative way to detect convection from space, but they lack the spatial and temporal resolution of ground-based observations. How-

ever, to use the observations, a sufficient localized filter is necessary to identify the MJO and other convective phenomena, such as Kelvin waves. There are currently various ways to identify waves and no universal index to use, which makes comparing studies difficult. In an effort to understand MJO initiation and its interaction with passing Kelvin waves, a localized index and unanimous wave filter is crucial. Advancements in the understanding of MJO initiation will be achieved with improvements in the time series of ground based observations, additional focus on satellite retrievals, and the establishment of a universal localized wave filter.

REFERENCES

Barrett, B. and L. M. Leslie, 2009: Links between Tropical Cyclone Activity and Madden-Julian Oscillation Phase in the North Atlantic and Northeast Pacific Basins. *Monthly Weather Review*, **137**, 727–744.

Blade, I. and D. L. Hartmann, 1993: Tropical intraseasonal oscillations in a simple nonlinear model. *Journal of Atmospheric Science*, **50**, 2922–2939.

Bond, N. A. and G. A. Vecchi, 2003: The Influence of the Madden-Julian Oscillation on Precipitation in Oregon and Washington. *Weather and Forecasting*, **18**, 600–613.

DYNAMO, 2011: DYNAMO Operations Plan. NSF, [Online], `http://www.eol.ucar.edu/projects/dynamo/documents/index.html`.

Fliegel, J., 2012: Quality Control and Census of SMART-R Observations from the DYNAMO/CINDY2011 Field Campaign. M.S. thesis, Dept. of Atmospheric Sciences, Texas A&M University, 84 pp.

Gill, A. E., 1980: Some simple solutions for heat-induced tropical circulation. *Quarterly Journal of the Royal Meteorological Society*, 447–462.

Google, 2013: Addu Atoll Map. Google, [Online], `google.maps.com`.

Gottschalck, J., P. E. Roundy, C. J. Schreck, A. Vintzileos, and C. Zhang, 2013: Large-Scale Atmospheric and Oceanic Conditions During the 2011-2012 DYNAMO Field Campaign. *Monthly Weather Review*, submitted.

Haertel, P. T. and G. N. Kiladis, 2004: Dynamics of 2-day equatorial waves. *Journal of the Atmospheric Sciences*, **61**, 2707–2721.

Hayashi, Y., 1970: A theory of large-scale equatorial waves generated by condensation heat and accelerating the zonal wind. *Journal of the Meteorological Society of Japan*, **48**, 140–160.

Houze, R. A., 2004: Mesoscale convective systems. *Reviews of Geophysics*, **42**, 43pp.

Hsu, H.-H., B. J. Hoskins, and F.-F. Jin, 1990: The 1985/86 intraseasonal oscillation and the role of the extratropics. *Journal of the Atmospheric Sciences*, **47**, 823–839.

Katsumata, M., R. H. Johnson, and P. E. Ciesielski, 2009: Observed Synoptic-Scale Variability during the Developing Phase of an ISO over the Indian Ocean during MISMO. *Journal of the Atmospheric Sciences*, **66**, 3434–3448.

Kemball-Cook, S. R. and B. C. Weare, 2001: The Onset of Convection in the Madden-Julian Oscillation. *Journal of Climate*, **14**, 780–793.

Lau, K.-M. and L. Peng, 1987: Origin of low-frequency (intra-seasonal) oscillations in the tropical atmosphere. Part I: Basic theory. *Journal of the Atmospheric Sciences*, **44**, 950–972.

Lau, K.-M., P.-J. Sheu, and I.-S. Kang, 1994: Multiscale low- frequency circulation modes in the global atmosphere. *Journal of the Atmospheric Sciences*, **51**, 1169–1193.

Lau, K.-M. and H.-T. Wu, 2010: Characteristics of Precipitation, Cloud, and Latent Heating Associated with the Madden-Julian Oscillation. *Journal of Climate*, **23**, 504–518.

Lindzen, R. S., 1974: Wave-CISK in the tropics. *Journal of the Atmospheric Sciences*, **31**, 156–179.

MacRitchie, K. and P. E. Roundy, 2012: Potential Vorticity Accumulation Following Atmospheric Kelvin Waves in the Active Convective Region of the MJO. *Journal of the Atmospheric Sciences*, **69**, 908–914.

Madden, R. A. and P. R. Julian, 1972: Description of global scale circulation cells in the Tropics with 40-50 day period. *Journal of the Atmospheric Sciences*, **29**, 1109–1123.

Madden, R. A. and P. R. Julian, 1994: Observations of the 40-50-day tropical oscillation - A review. *Monthly Weather Review*, **122**, 814–837.

Majda, A. J. and J. A. Biello, 2004: A multiscale model for tropical intraseasonal oscillation. *Proceedings of the National Academy of Sciences USA*, **101**, 4736–4741.

Masunaga, H., 2007: Seasonality and Regionality of the Madden-Julian Oscillation, Kelvin Wave, and Equatorial Rossby Wave. *Journal of the Atmospheric Sciences*, **64**, 4400–4416.

Masunaga, H., 2009: A 9-season TRMM Observation of the Austral Summer MJO and Low-frequency Equatorial Waves. *Journal of the Meteorological Society of Japan*, **87A**, 295–315.

Masunaga, H., T. S. L'Ecuyer, and C. D. Kummerow, 2006: The Madden-Julian Oscillation Recorded in Early Observations from the Tropical Rainfall Measuring Mission (TRMM). *Journal of the Atmospheric Sciences*, **63**, 2777–2794.

Nakazawa, T., 1988: Tropical super clusters within intraseasonal variations over the western Pacific. *Journal of the Meteorological Society of Japan*, **66**, 823–836.

Roundy, P. E., 2008: Analysis of Convectively Coupled Kelvin Waves in the Indian Ocean MJO. *Journal of the Atmospheric Sciences*, **65**, 1342–1359.

Schreck, C. J., 2013: Monitoring the MJO and Tropical Waves. C. J. Schreck, [Online], `http://monitor.cicsnc.org/mjo/current/`.

Seo, K.-H. and K.-Y. Kim, 2003: Propagation and initiation mechanisms of the Madden-Julian oscillation. *Journal of Geophysical Research*, **108**, 4384–4405.

Sobel, A. H., S. E. Yuter, C. S. Bretherton, and G. N. Kiladis, 2004: Large-Scale Meteorology and Deep Convection during TRMM KWAJEX. *Monthy Weather Review*, **132**, 422–444.

Steiner, M., J. R. A. Houze, and S. E. Yuter, 1995: Climatological Characterization of Three-Dimensional Storm Structure from Operational Radar and Rain Gauge Data. *Journal of Applied Meteorology*, **34**, 1978–2007.

Straub, K. H. and G. N. Kiladis, 2002: Observations of a convectively coupled kelvin wave in the eastern Pacific ITCZ. *Journal of the Atmospheric Sciences*, **59**, 30–53.

Straub, K. H. and G. N. Kiladis, 2003: The observed structure of convectively coupled kelvin waves: Comparison with simple models of coupled wave instability. *Journal of the Atmospheric Sciences*, **60**, 1655–1668.

Swann, A., A. H. Sobel, S. E. Yuter, and G. N. Kiladis, 2006: Observed radar reflectivity in convectively coupled Kelvin and mixed Rossby-gravity waves. *Geophysical Research Letters*, **33**.

Webster, P. J. and R. Lukas, 1992: TOGA COARE: The Coupled Ocean-Atmosphere Response Experiment. *Bulletin of the American Meteorological Society*, **73**, 1377–1416.

Wheeler, M. C., 2013: Monitoring and Prediction of Modes of Coherent Tropical Variability. M. C. Wheeler, [Online], `http://cawcr.gov.au/staff/mwheeler/maproom/OLR_modes/index.htm`.

Wheeler, M. C. and H. H. Hendon, 2004: An All-Season Real-Time Multivariate MJO Index: Development of an Index for Monitoring and Prediction. *Monthly Weather Review*, **132**, 1917–1932.

Wheeler, M. C. and G. N. Kiladis, 1999: Convectively coupled equatorial waves: Analysis of clouds and temperature in the wave-number-frequency domain. *Journal of the Atmospheric Sciences*, **53**, 449–467.

Yamada, H., K. Yoneyama, M. Katsumata, and R. Shirooka, 2010: Observations of a Super Cloud Cluster Accompanied by Synoptic-Scale Eastward-Propagating Precipitating Systems over the Indian Ocean. *Journal of the Atmospheric Sciences*, **67**, 1456–1473.

Yamasaki, M., 1969: Large-scale disturbances in the conditionally unstable atmosphere in low latitudes. *Papers in Meteorology and Geophysics*, **20**, 289–336.

Yanai, M., B. Chen, and W. W. Tung, 2000: The Madden-Julian Oscillation observed during the TOGA COARE IOP: Global View. *Journal of the Atmospheric Sciences*, **57**, 2374–2396.

Yarnal, B., 1993: *Synoptic Climatology in Environmental Analysis*. Belhaven Press.

Yoneyama, K., Y. Masumoto, Y. Kuroda, M. Katsumata, K. Mizuno, and Coauthors, 2008: MISMO FIELD EXPERIMENT IN THE EQUATORIAL INDIAN OCEAN. *Bulletin of the American Meteorological Society*, 1889–1903.

Zhang, C., 2005: Madden-Julian Oscillation. *Reviews of Geophysics*, **43**.

Zuluaga, M. D. and R. A. Houze, 2013: Evolution of the Population of Precipitation Convective Systems over the Equatorial Indian Ocean in Active Phases of the Madden-Julian Oscillation. *Journal of the Atmospheric Sciences*, submitted.